photonics

MDPI

Review

Physical and Technological Aspects of Laser-Induced Damage of ZGP Single Crystals under Periodically Pulsed Laser Irradiation at 2.1 μm

Nikolay Yudin N. Yudin [1,2,*], Victor Dyomin [1], Alexander Gribenyukov [3], Oleg Antipov [2], Andrei Khudoley [4], Igor O. Kinyaevskiy [5], Mikhail Zinovev [1], Sergey Podzyvalov [1], Vladimir Kuznetsov [1], Elena Slyunko [1], Alexey Lysenko [1], Andrey Kalsin [1], Ilya Eranov [2] and Houssain Baalbaki [1]

[1] Laboratory of Radiophysical and Optical Methods for Studying the Environment, Radiophysics Department, National Research Tomsk State University, 634050 Tomsk, Russia; dyomin@mail.tsu.ru (V.D.); muxa9229@gmail.com (M.Z.); cginen@yandex.ru (S.P.); robert_smith_93@mail.ru (V.K.); elenohka266@mail.ru (E.S.); festality@yandex.ru (A.L.); andrejkalsin@gmail.com (A.K.); houssainsyr1@gmail.com (H.B.)

[2] Institute of Applied Physics of the Russian Academy of Sciences, 603950 Nizhny Novgorod, Russia; antipov@ipfran.ru (O.A.); 72ilya305@mail.ru (I.E.)

[3] Technological Laboratory, Institute of Monitoring of Climatic and Ecological Systems, Siberian Branch, Russian Academy of Sciences, 634055 Tomsk, Russia; alexander.gribenyukov@yandex.ru

[4] Institute of Heat and Mass Transfer Named after A.V. Lykov NAS of Belarus, 220072 Minsk, Belarus; khudoley@hmti.ac.by

[5] Physical Institute of the Russian Academy of Sciences, 119991 Moscow, Russia; kinyaevskiyio@lebedev.ru

* Correspondence: rach3@yandex.ru; Tel.:+7-996-938-7132

Abstract: The nonlinear properties of zinc germanium diphosphide (ZGP) crystals enable their applications in powerful mid-IR optical parametric oscillators and second-harmonic generators. This paper summarizes the mechanisms of the laser-induced damage (LID) of high-purity ZGP crystals under periodically pulsed nanosecond irradiation by a Ho^{3+}:YAG laser at 2.1 μm. The ZGP samples were manufactured by "LOC" Ent., Tomsk, Russia, or the Harbin Institute of Technology, China. The impact of processing techniques and the post-growing methods for polishing and anti-reflective coatings on the LID threshold are discussed. The importance of the defect structure of the crystal lattice and the parameters of transparent coatings for increasing the LID threshold are also discussed. The impact of the test laser parameters on the LID threshold and the transient area near the LID threshold obtained using digital holography are analyzed. The influence of the pre-damage processes on the optical parametric oscillations is reported. Lastly, the prospects for improving ZGP crystals to further increase the LID threshold are discussed.

Keywords: ZGP; single crystal; laser-induced damage threshold; mid-IR optical parametric oscillators and generators; Ho^{3+}:YAG lasers

Citation: Yudin, N.Y.N.; Dyomin, V.; Gribenyukov, A.; Antipov, O.; Khudoley, A.; Kinyaevskiy, I.O.; Zinovev, M.; Podzyvalov, S.; Kuznetsov, V.; Slyunko, E.; et al. Physical and Technological Aspects of Laser-Induced Damage of ZGP Single Crystals under Periodically Pulsed Laser Irradiation at 2.1 μm. *Photonics* **2023**, *10*, 1364. https://doi.org/10.3390/photonics10121364

Received: 10 October 2023
Revised: 21 November 2023
Accepted: 24 November 2023
Published: 11 December 2023

1. Introduction

Periodically pulsed sources of powerful coherent mid-infrared (mid-IR) radiation have a wide range of applications in many areas of science and technology. In particular, frequency converters operating in the 3.5–5 μm and 8–12 μm wavelength ranges are promising for optical communications in the atmosphere within the framework of global 6G-generation information transmission systems [1]. Sources of coherent mid-IR radiation are also used for processing materials (glasses, ceramics, or semiconductors) by scribing and thermal splitting [2,3] and in medicine, during disease diagnosis using gas analysis and the resonant ablation of biological tissues due to their strong water and collagen absorptions [4–9]. Sources of coherent radiation capable of generating powerful pulsed radiation in the 3.5–5 μm wavelength range are relevant for the creation of lidar systems

based on the method of differential absorption for greenhouse gas emission control (since the most intense absorption lines of most greenhouse gases lie in this spectral range) [10–13]. One of the most efficient solid-state sources of coherent radiation in the mid-IR range are optical parametric oscillators (OPOs) and optical parametric generators and amplifiers (OPGs and OPAs).

The most powerful OPOs in the important mid-IR windows are currently based on nonlinear-optical $ZnGeP_2$ (ZGP) crystals [14–16]. These OPOs are pumped by the well-established Q-switched Ho^{3+}:YAG lasers at 2.1 μm and are capable of high-efficiently generating at 3.5–5 μm, with an average power of up to 160 W or pulse energy of up to 200 mJ at a pulse width of 10–60 ns and repetition rate from a few Hz to 100 kHz [17–22]. Moreover, the Ho^{3+}:YAG laser-pumped OPOs based on $ZnGeP_2$ crystals operate efficiently at wavelengths 6–7 μm, 8.1–8.3 μm, and 9–10 μm [23–26]. The ZGP crystals used for mid-IR OPGs and OPAs in broadband laser systems were also able to generate ultra-short picosecond and femtosecond pulses [15,27–30]. However, the prolonged operation of powerful OPOs and OPGs/OPAs based on ZGP is limited by the laser-induced damage (LID) of this material. In accordance with the results of numerous studies [31–48], the ZGP LID always occurs at the sample surface or in the sub-surface layer rather than in the bulk in samples subjected to repetitively pulsed nanosecond-pulse-width infrared radiation. A combination of factors associated with defects in the crystal structure in the sub-surface layer and the quality of polishing of the surface itself affects the LID. In this regard, the potential for the practical use of optical parametric devices in the mid-IR range is associated, in particular, with the need to improve the methods of synthesis, growth, and processing of the working surfaces of the ZGP crystals in order to increase their LID threshold (LIDT).

There have been a number of publications on the problem of the ZGP LID induced by lasers operating at wavelengths from 1.064 μm to 10 μm [31–48]. These studies have revealed a significant difference in the LIDT of ZGP crystals at wavelengths of 1.064 μm and 2.1 μm [31]. Dynamic visualization of the breakdown process initiated by laser radiation at 2.1 μm in ZGP crystals showed that the optical damage of a single ZGP crystal under nanosecond repetitively pulsed radiation is mainly initiated by thermal effects [32]. The increase in the ZGP LIDT with a decrease in the pulse width of the pump radiation reported in [33] also "supports the thermal nature of the breakdown for nanosecond pulses due to anomalous infrared absorption." In [35], it was reported that a ZGP LIDT of 9.55 μm was determined by the intensity of an incident beam of 142 MW/cm^2 at a pulse duration of 85 ns and a repetition rate of 1 Hz, which is ~9.5 J/cm^2 in terms of the pulse energy density. A direct dependence of the LIDT on the growth technology and optical quality of crystals was also demonstrated in [34].

In [40], it was shown that the LIDTs measured on ZGP samples with an anti-reflection (AR) coating are much lower compared to samples without a coating. In [37], it was shown that the application of AR interference coatings led to a twofold increase in the LIDT. In [41], the authors concluded that, in order to increase the output power and efficiency of parametric frequency conversion in the ZGP crystal in the spectral range of 3–5 μm, further research should be focused on improving the quality of AR coatings using a high-quality ZGP crystal.

The conflicting information about the effect of interference coatings on the ZGP LIDT presented in [37,40] suggests that the different design of coatings and methods of their application on a nonlinear crystal significantly affects the efficiency of its use in OPOs. In [42–45], comprehensive studies were conducted on the influence of the parameters of the application of AR coatings and film-forming materials on the ZGP LIDT under mid-IR laser irradiation with femtosecond, picosecond, and nanosecond pulse durations.

In [34,37,38], it was shown that improving the polishing of ZGP working surfaces and either reducing or completely removing the near-surface crack layer leads to an increase in the LIDT. In [37,38], when the near-surface crack layer was reduced, Rq was reduced by half and the PV parameter changed by more than five times, while the optical breakdown threshold by energy density increased two times. The LIDT at a wavelength of 2.05 μm

and a pulse repetition frequency (PRR) of 10 kHz for ZGP samples with a deposited anti-reflection coating was improved from 1 J/cm^2 to 2 J/cm^2. The increase in LIDT was achieved by improving the polishing of the surface of the ZGP samples. At the same time, the research results presented in [34] showed no changes in the LIDT when the polishing parameter Rz was almost the same but the Rq parameter was changed over four times and the Ra parameter by more than five times. It was suggested that it is the roughness of the polished surface (peaks and valleys), described by the Rz parameter, that contributes to the mechanism of optical breakdown and can be "seeding" inhomogeneities for the initiation of optical breakdown due to field effects at a wavelength of 2091 nm.

One of the most promising methods for improving surface quality is magnetorheological polishing [46], which is increasingly being used in the processing of laser crystals to improve the threshold of radiation resistance and reduce the level of roughness. In [47], magnetorheological processing was first used for polishing the working surfaces of a single ZGP crystal. A non-aqueous liquid with magnetic particles of carbonyl iron, with the addition of nanodiamonds, was used in the process. This enabled samples of a single ZGP crystal with a surface roughness level measured in angstroms. The use of magnetorheological polishing made it possible to more accurately characterize the possible structural defects, with a size of ~0.5–1.5 μm, that appeared on the surface of a single crystal. The value of the LIDT caused by the laser at the specified surface roughness parameters was determined not by the quality of polishing, but by the number of point recesses caused by the physical limitations of the structural configuration of the crystal volume. These results are in good agreement with the assumption about the significant influence of the dislocation concentration in the ZGP crystal on LIDT put forward in [48]. Despite the fact that the sample subjected to MRP showed a significant improvement in the surface roughness parameters compared to the sample polished using traditional technology, the LIDT practically did not change. The absence of a difference in the LIDT for the two samples was due to the physical limitations of the structural configuration of the crystal.

Based on the data provided in Table 1, the LIDT of our tested ZGP samples can be affected by the structural imperfection and impurity composition of the crystal, the quality of the crystal's working surfaces, as well as the external factors that include the parameters of the testing laser radiation and crystal temperature.

Note that the discrepancies between different interpretations of experimental ZGP LID data indicate several possible scenarios of damage spot formation, even at the same wavelength and pulse width. This fact is an indication of several complex mechanisms that include the combination of thermal damage and field-induced optical breakdown, physical effects (such as photoionization to or from impurity levels, multi-stage excitation, the generation of free carriers with subsequent avalanche ionization, the formation of electron-hole solid-state plasma with increasing optical absorption, the nonlinear dependence of the thermo-optical parameters, etc.) and dynamic peculiarities (such as accumulation effects and multiple-pulse material degradation) associated with the LID of the high-transmitting dielectric crystals irradiated with nanosecond laser pulses at a high PRR [49,50]. In contrast, a more defined dominant LID mechanism for the longer pulses (with a microsecond or more pulse width) is the thermal effect related to the melting and/or vaporization of the material. The field-induced breakdowns of the crystal surfaces, multiphoton absorption, and avalanche ionization under super-high intensity irradiation can be the main LID-initiation effects for the ultra-short picosecond or sub-picosecond pulses without the accumulation effects that occur at a high PRR [49,51].

This paper will give an overview of the research conducted to determine the contribution of each of the factors listed above to the value of the LIDT. The tested ZGP samples were manufactured by "LOC" Ent., Tomsk, Russia, or the Harbin Institute of Technology (HIT), Harbin, China. The single-crystalline ZGP samples had high purity and structural perfection [34,48]. The repetitively pulsed Ho^{3+}:YAG lasers at 2097 nm pumped by a Tm fiber laser at 1908 nm were used for the LID tests [52]. The tests were performed at a wavelength of 2097 nm due to the common use of the high-power repetitively pulsed

Ho^{3+}:YAG lasers as the pumping source of the ZGP-based mid-IR OPOs. The "R-on-1" method was applied for all ZGP LIDT tests [53].

Table 1. Summary of the data on ZGP crystals and the laser parameters in the LID tests.

Absorption at the Exposure Wavelength, cm^{-1}	Dopant	Crystal Length, mm	Coating	Wavelength, μm	Pulse Repetition Rate, kHz	Pulse Width, ns	Test Time, s	Beam Diameter, μm	Temperature, °C
	-	2.2	No	2.091	1	21	30	200	room
1.8	-	2,2	No	1.064	0.1	8	30	280	room
0.03	-	20	SiO_2/Nb_2O_5	2.091	12	18	1	270	room
0.03	-	20	SiO_2/Nb_2O^5	2.091	12	18	1	100	−60
7.5	-	2.45	No	1.064	3	10	1	-	room
0.26	-	-	No	9.55	0.001	85	-	-	room
-	-	-	No	2.08	0.001	70–75	-	750	room
-	-	-	With coating	2.05	10	15	30	130	room
	Se	2.45	No	2.097	10	35	10	360	room
	Mg	2.45	No	2.097	10	35	10	360	room
	Ca	2.45	No	2.097	10	35	10	360	room
-	-	20	$ZnSe/Al_2O_3$	2.097	10	35	10	350	room
0.03	-	20	YbF_3/ZnS	2.097	10	35	10	350	room
0.03	-	20	ZnS/Al_2O_3	2.097	10	35	10	350	room
-	-	2.45	-	1.03	Single pulse mode	0.0003–0.003	-	-	room
0.03	-	20	No	2.097	10	35	10	350	room
-	-	3	No	2.091	40	45	1	270	room

2. The Effect of the Defect Structure of the ZGP Crystal Lattice on the LIDT Value

The effect of the ZGP structure on the LIDT was tested in the first series for the samples manufactured by the Harbin Institute of Technology. The first tested element with dimensions of $6 \times 6 \times 20$ mm^3 was cut from a ZGP crystal grown in the year 2012 (sample N1). The axis of the sample N1 element was oriented at angles of $\theta = 57.2^\circ$ and $\varphi = 0^\circ$ with respect to the crystal optical axis.

The second tested elements with dimensions of $6 \times 6 \times 3$ mm^3 (two plates) were cut from a novel ZGP crystal grown in the year 2020 (samples N2). The sample N2 elements were cut at angles $\theta = 57.2^\circ$ and $\varphi = 0^\circ$ with respect to the crystal optical axis.

The ZGP crystals, sample N1 and sample N2, were grown under different technological conditions: their growth rates were 0.8 mm/h and 0.3 mm/h and their temperature gradients were 9.0 K/cm and 5.0 K/cm for sample N1 and sample N2 ZGP crystals, respectively. The different growth parameters resulted in a difference in the LIDT of the ZGP crystals. In our previous reports, the main types of defects detected by X-ray topography in ZGP crystals were macroscopic stress fields, dislocations, growth striate, and microdefects [54,55]. The different growth parameters resulted in the difference in the quality of the ZGP crystals. The high quality of the crystal is attributed to the high LIDT. The sample N2 was grown more recently under improved growth conditions, attributing to it higher structural perfection and a smaller density of inclusions, free from twins and stacking faults. Instead, sample N1 had macroscopical bends, tilting of blocks and twins, and a high density of dislocations. The average dislocation density in the samples studied decreased from $N_{dis} \approx 6 \times 10^4$ cm^{-2} to $N_{dis} \approx 6 \times 10^3$ cm^{-2}. As shown in Figure 1, the ZGP samples (both the sample N1 and sample N2 elements) were polished to fit laser optic quality requirements (PV ≈ 55 nm and RMS ≈ 10 nm). For the artificial polished samples, the roughness and the flatness were less than 0.233 nm and 0.683λ (at wavelength λ = 632.8 nm), respectively.

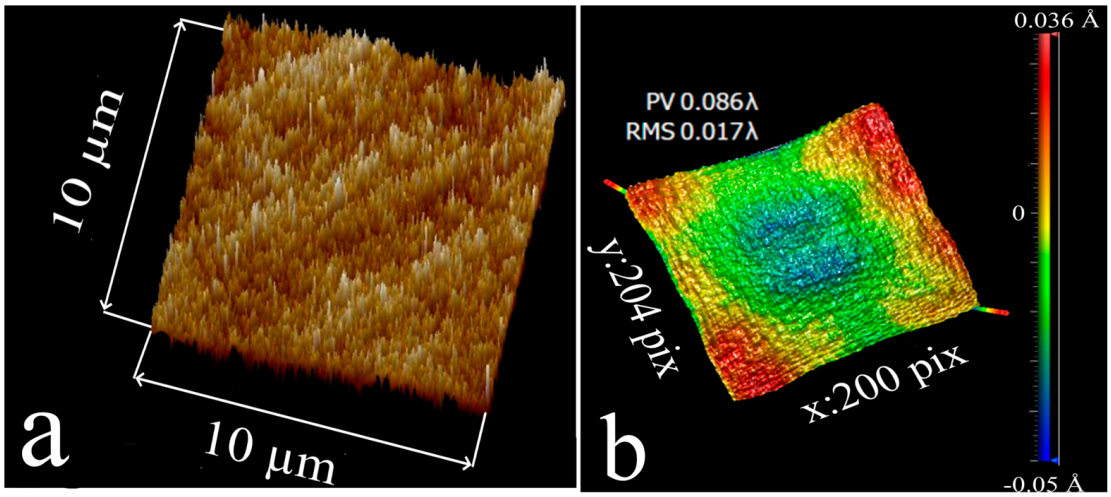

Figure 1. Patterns of the roughness and flatness of the ZGP elements, registered by a ZYGO interferometer, surface relief (**a**); surface roughness (**b**) (adapted from [48]).

The probability of the optical damages of the sample N1 and sample N2 elements were compared at the same parameters of the experiments (PRR, pulse width, and exposure duration) (Figure 2).

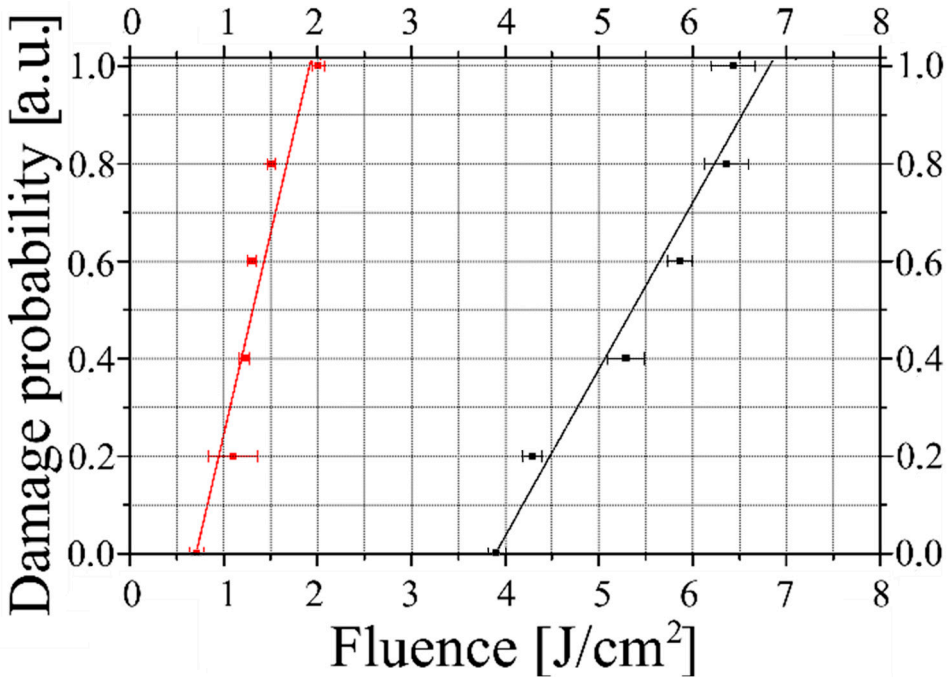

Figure 2. Comparison of the probability of the optical damage of the sample N1 element (red squares) and the sample N2 element (black squares) at 12 kHz PRR, 1 s exposure duration, pulse width of 18 ns, and beam diameter of 360 μm (adapted from [48]).

The comparison of the experimental results and the calculated statistical parameters demonstrated a four times higher LIDT (both the average fluence and the 0-probability LIDT fluence) for sample N2 in comparison with sample N1 (Figure 2).

The critical values of the pulse fluence, peak, and average power were measured to be much higher for the sample N2 elements compared to the sample N1 elements. It is well known that the ZGP LIDT depends on surface polishing [31,34,37,38].

The LIDs of the ZGP samples (manufactured by HIT or LOC) were comparatively examined by the same R-on-1 test method and at the same test conditions: the testing laser

wavelength was ~2.1 μm and the PRR was 10–12 kHz. The pulse width and the beam diameter of the Ho^{3+}:YAG laser were 18 ns or 35 ns and 180 μm or 350 μm (at the e^{-2} level of the maximum intensity) for the HIT or LOC samples, respectively [44,48]. The measured ZGP LIDT for the pulse fluence was 3.45 J/cm^2 or 3.9 J/cm^2 for the LOC or HIT samples.

It was experimentally found that the change in the crystal growth technology resulted in the biggest increase in the LIDT. The growth conditions resulted in a high lattice quality with a low occurrence of impurities. The improved growth technology also led to a reduced number of microdefects and a more uniform distribution of dislocations. This, in turn, resulted in higher optical homogeneity and a higher LIDT of the material.

Various crystal impurities can affect the surface LIDT, both decreasing and increasing it. Recently, the effect of the annealing atmosphere of chalcogenide crystals with the presence of Ar, Se, and Zn on the mid-IR LIDT was reported [56]. For our presented study on the influence of the impurity composition on the LIDT, a single ZGP crystal (manufactured by LOC) was used, from which eight samples were cut with (100) orientation and dimensions 5 × 5 × 2.45 mm^3. Mg, Se, and Ca were thermally sputtered onto the pre-polished faces of the samples (the thickness of the sprayed film was 1 μm). After that, the ZGP samples with deposited films and two control samples without deposition were annealed in a sealed evacuated ampoule, into which a weighed amount of ZGP powder was added, at a temperature of 650 °C for one set of samples and at 750 °C for another similar set for 180 h. After diffusion doping, the working surfaces of the test samples were re-polished. The LID of the obtained ZGP samples was tested by the following parameters of the Ho^{3+}:YAG laser: the pulse width was 35 ns, the PRR was 10 kHz, and the laser beam diameter at the input surface of the studied samples was 350 ± 10 μm, similar as in the above-described experiments.

The results of measuring the LIDT of the ZGP samples annealed at temperatures of 650 °C and 750 °C without doping and with doping of Mg, Se, and Ca using the R-on-1 method are shown in Figure 3.

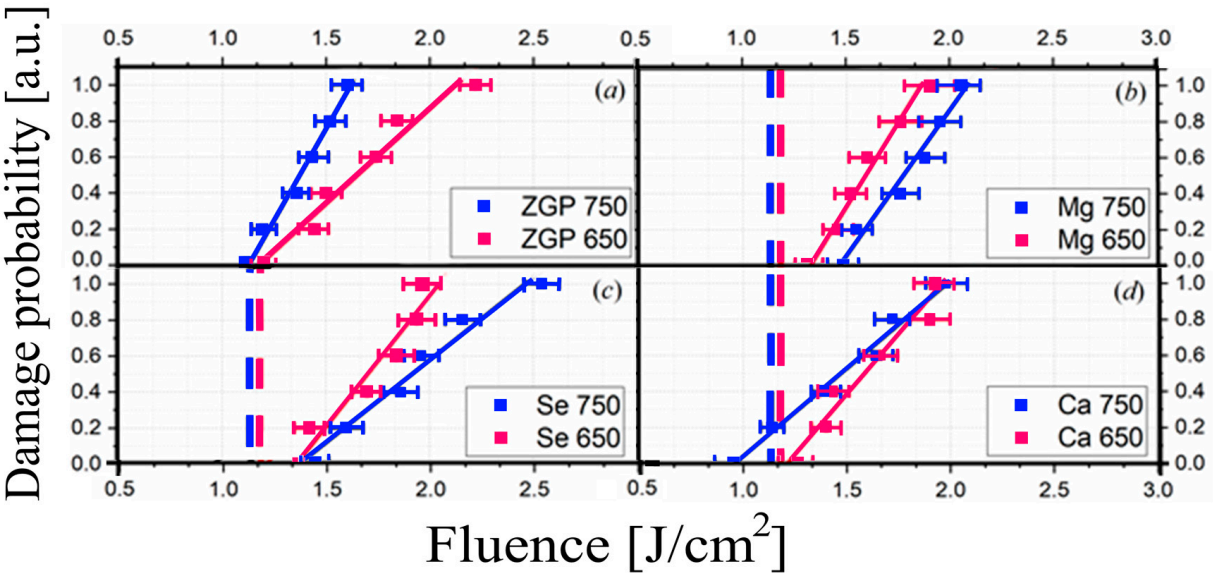

Figure 3. Dependence of the probability of optical damage on the energy density of the incident laser radiation with a wavelength of 2.1 μm in undoped samples (**a**), and in doped samples with Mg (**b**), Se (**c**), and Ca (**d**). Approximate plots in black and red correspond to ZGP samples annealed at 750 °C and 650 °C, respectively (adapted from [39]).

In the undoped samples (Figure 3a), there were no significant changes in the LIDT (the detected changes were within the measurement error) depending on the annealing temperature, which is in good agreement with the results of [34]. At the same time, in samples doped with Mg or Se by diffusion, after annealing at a temperature of 650 °C, the

LIDT increased by 15% and 17%, respectively. When annealing at a temperature of 750 °C, the LIDT of samples doped with Mg and Se increased by 31% and 21%, respectively. An inverse dependence was observed for the sample doped with Ca. When annealing at a temperature of 650 °C, LIDT changes were not found, and when annealing at a temperature of 750 °C, the damage threshold decreased by 14%. The presented results indicate a qualitative tendency for the LIDT to decrease or increase depending on the concentration of the doped material. It should be noted that for doped samples with Mg and Se, there was a tendency for the LIDT to increase with increasing dopant concentration (since samples annealed at 750 °C had a higher optical damage threshold than samples annealed at 650 °C). An inverse dependence was observed for the samples doped with Ca by diffusion. The best results were the results of the single crystal ZGP doped with Mg at a temperature of 750 °C.

From the results of measuring the LIDT and electrical conductivity (Table 2), a qualitative dependence can be seen. Doping with chemical elements caused a decrease in the electrical conductivity of the samples (σ) and led to an increase in the LIDT, and vice versa, doping with chemical elements caused an increase in the electrical conductivity of the samples and led to a decrease in the LIDT. For example, when ZGP crystals are doped with calcium, σ increases by about an order of magnitude, while, on the contrary, when ZGP is doped with Mg and Se, σ decreases by about an order of magnitude.

Table 2. Conductivity and LIDT of the studied ZGP samples.

Dopant	Conductivity, (ohm × cm)$^{-1}$	LIDT of the Samples Annealed at 650 °C, J/cm^2	LIDT of the Samples Annealed at 750 °C, J/cm^2
Mg	$(5.42 \pm 0.01) \times 10^{-6}$	2.6 ± 0.1	2.9 ± 0.1
Se	$(4.16 \pm 0.01) \times 10^{-7}$	2.64 ± 0.1	2.7 ± 0.1
Ca	$(1.25 \pm 0.01) \times 10^{-5}$	2.28 ± 0.1	1.9 ± 0.1
ZGP	$(1.24 \pm 0.01) \times 10^{-6}$	2.26 ± 0.1	2.2 ± 0.1

From the presented data in Table 2, diffusion doping with various chemical elements leads to an increase or decrease in the LIDT.

The LID in semiconductor materials at a nanosecond pulse width can be a consequence of direct thermal effects or the electric-field-induced processes associated with the generation of electron-hole plasma [49,50]. A local increase in temperature near small crystalline defects and inclusions under the pulsed radiation can initiate LID. Indeed, point defects in a crystal lattice can enhance, for example, additional electronic sublevels, which facilitate multiphoton absorption at 2.09 μm and a sharp increase in temperature. The dislocation regions located inside the ZGP, especially near the surface of the sample, accumulate a number of point defects and inclusions, which provide an increase in temperature to a critical value. On the other hand, the local electric field at the dislocation point is stronger than in a homogeneous lattice, which leads to a lower LIDT, enhanced by the electric field [34,48]. Thus, it becomes obvious that the decrease in the conductivity of ZGP crystals doped with Mg and Se should contribute to an increase in the LIDT.

3. The Effect of ZGP Anti-Reflection Coatings on LIDT

Comprehensive studies of the influence of the deposition parameters of AR interference coatings and film-forming materials on the LIDT of ZGP samples (manufactured by LOC) under Ho^{3+}:YAG laser irradiation have been performed [42–45]. The coatings were achieved with an Aspira-200 vacuum deposition machine by ion beam sputtering (IBS). The maximum diameter of the targets was 101.6 mm and the thickness of each was up to 10 mm. The gas supply system had electronic flow meters and valves. The system was supplied with gases—ultra-pure argon (Ar 99.999%) and technical pure oxygen (O_2 99.7%). The ion source was an accelerator with an anodic layer. Control of the gas parameters and control of the ion source parameters was carried out from the control computer of the vacuum

installation. Compensation of the positive charge formed on the target surface during sputtering was performed using the thermos-emission of electrons from a heated tungsten cathode. Before loading into the deposition chamber, the substrates were cleaned using ultra-pure acetone and then washed with distilled water. Immediately before applying the coating in the vacuum chamber, the substrates were additionally cleaned with an auxiliary ion source at a source power of ~40 W and ion energy of ~150 eV for 10 min. The substrate temperature was maintained at 100 °C throughout the entire deposition process.

Using the specified technology, AR coatings for various pairs of film-forming materials were developed. Information on the coating materials and their parameters is given in Table 3. For clarity, a histogram of the LIDT of ZGP crystals, depending on the type of AR coating, is shown in Figure 4.

Table 3. Pairs of film-forming materials and AR coating parameters and the LIDT fluence.

Sample	LIDT Fluence, J/cm^2	Coating Thickness, nm	Number of Layers
Nb_2O_5/SiO_2_1	1.8	2900	5
Nb_2O_5/Al_2O_3	2.35	2133	3
ZnS/Al_2O_3	3.45	825	3
Nb_2O_5/SiO_2_2	1.86	700	4
YbF_3/ZnS	2.9	1305	7
$ZnSe/Al_2O_3$	3.51	721	3

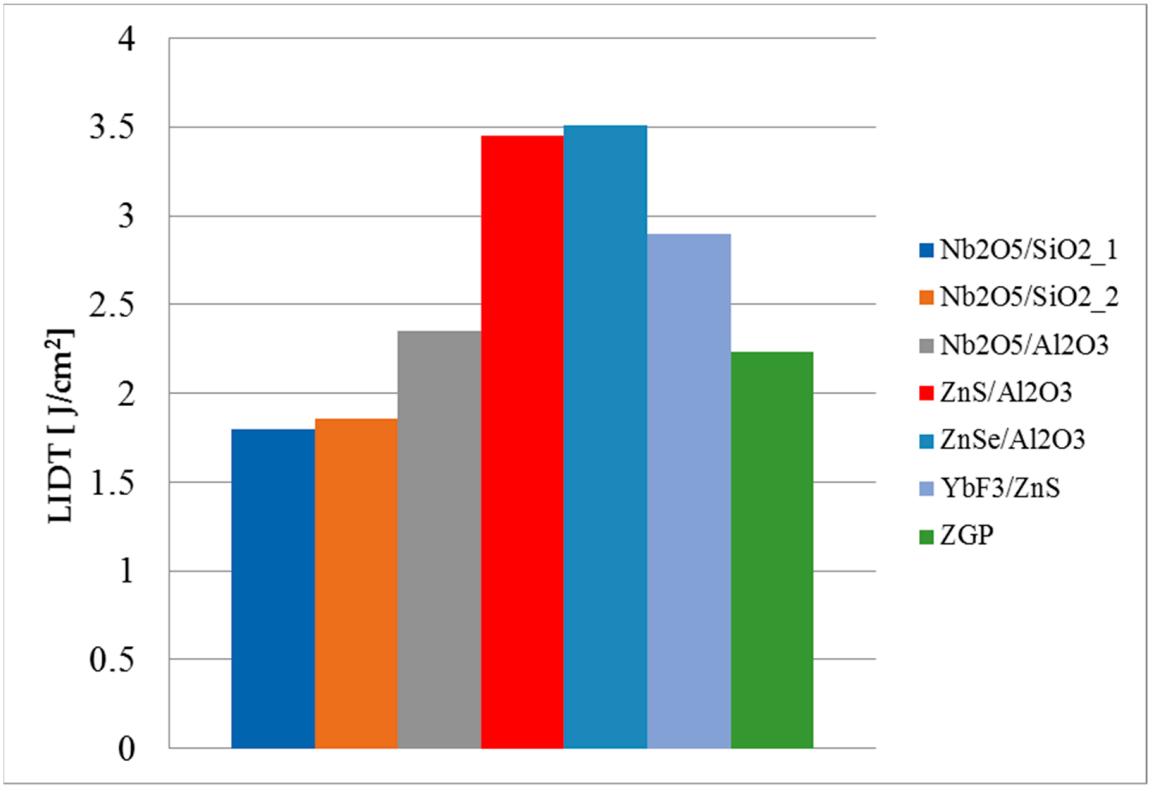

Figure 4. Histogram of the LIDT value depending on the type of AR coating.

From the results presented in Figure 4 and Table 3, which are the result of summarizing the information obtained in [42–45], the following patterns can be observed:

1. The smaller the thickness of the AR coating, the higher the LIDT under otherwise equal conditions (deposition regimes and film-forming materials);

2. The magnitude of the radiation resistance of ZGP crystals with a deposited AR coating is significantly affected by the optimal selection of a pair of film-forming materials (it is necessary that the mechanical properties of the coating layers be close to the properties of the ZGP substrate).
3. The optimal deposition conditions for AR coatings allow for a reduction in the number of film defects and an increase in the LIDT.

As can be seen from the results presented in Table 3 and Figure 4, it is possible to increase the LIDT of ZGP by 50%, compared to uncoated samples, by optimizing the parameters for the AR coatings, when applying interference coatings based on pairs of ZnS/Al_2O_3 and $ZnSe/Al_2O_3$ materials.

4. Effect of External Factors on the LIDT of ZGP Crystals

The effects of laser exposure duration and laser beam diameter on the LIDT of a ZGP crystal at room temperature as well as the effect of crystal temperature on LIDT were studied [34]. The Ho^{3+}:YAG laser with a radiation of 2091 nm with 12 kHz PRR and 18 ns pulse width was used.

It was shown that with an increase in exposure duration from 2 to 30 s, the LIDT decreases by 1.2 times, from 1.57 to 1.28 J/cm^2 (Figure 5).

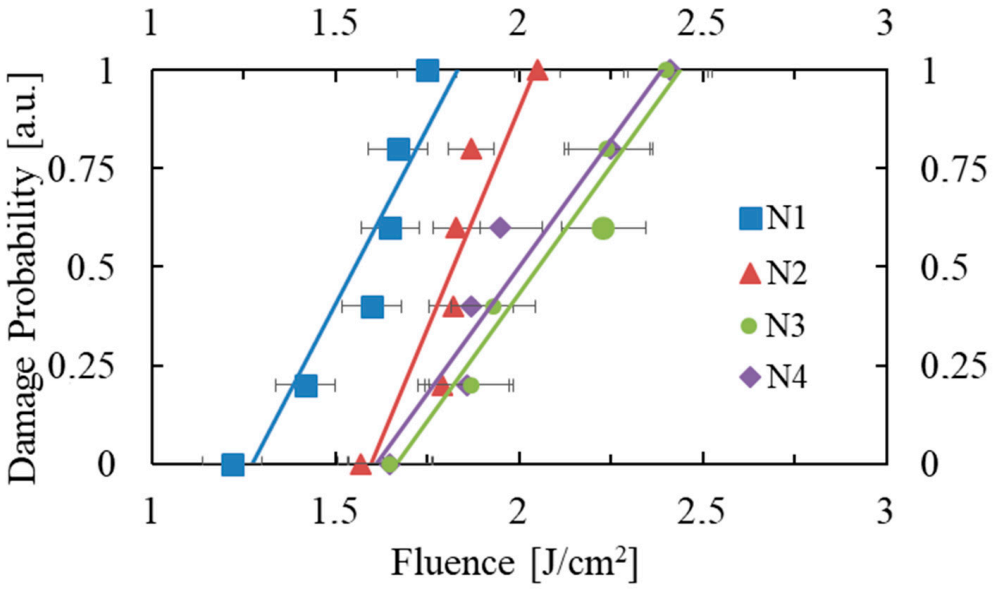

Figure 5. Dependence of the probability of optical damage on the fluence of laser radiation at 2091 nm for various exposure times τ_{ex}: 30 s (N1), 10 s (N 2), 5 s (N 3), and 2 s (N 4) (adapted from [34]).

Measurements at room temperature showed that when the diameter of the test laser beam becomes smaller, the LIDT increases, i.e., when the diameter of the beam was reduced by 2.9 times from 580 to 200 μm (at the level of e^{-2}), W_{0d} increased 1.4 times from 1.32 to 1.91 J/cm^2 (Figure 6).

The increase in LIDT, with a decrease in the diameter of the laser beam, and the decrease in LIDT, with an increase in exposure time, can be explained by the thermal effects when the crystal is exposed to radiation at 2091 nm.

To study the temperature dependence of the LIDT, in [34], the ZGP samples were placed in a sealed cuvette filled with dry nitrogen at normal pressure. Using a calorimetric cup filled with liquid nitrogen and having thermal contact with the cuvette, the sample was cooled to a temperature of −106 °C (the sample temperature was controlled by an electronic thermometer). The windows of the cuvette were made of crystalline sapphire without AR coatings with a transmission coefficient (at 2091 nm) of ≈85%. The incident laser beam was focused onto the front face of the ZGP onto a spot with a diameter of d ≈ 100 μm and a spot with a diameter of d ≈ 270 μm.

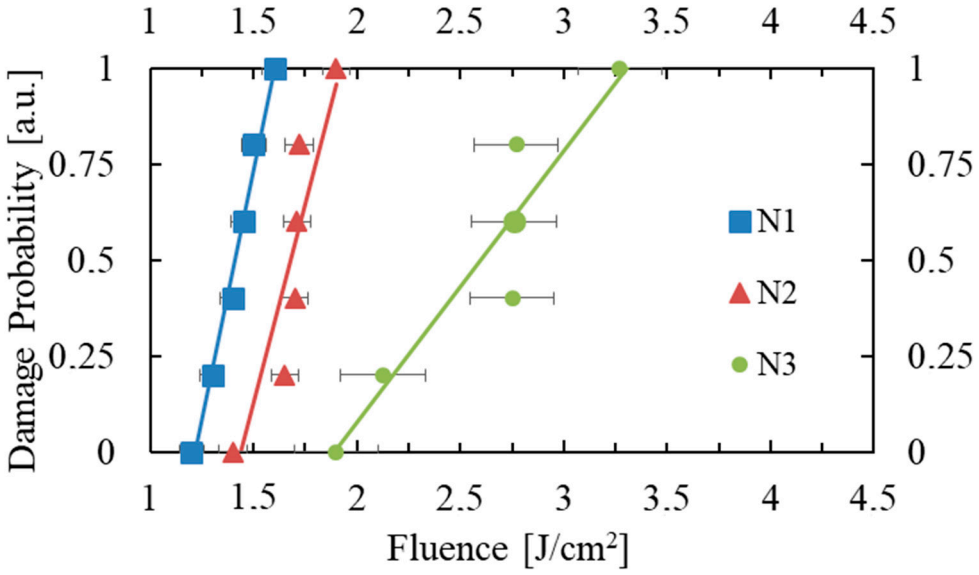

Figure 6. Dependence of the LID probability on the laser fluence at 2091 nm for various beam diameters: 580 μm (N 1), 300 μm (N 2), and 200 μm (N 3) (adapted from [34]).

At room temperature and with a laser beam diameter of 270 μm, the threshold breakdown values for the ZGP sample were W_{0d} = 2.3 J/cm^2 and W_D = (3.4 ± 0.4) J/cm^2. The measurement results demonstrated a significant increase in the LIDT, especially noticeable when the temperature was reduced from 20 °C to −60 °C (Figure 7a). In the temperature range from +24 to −86 °C with a laser beam diameter of 100 μm, a more than three times (from 3.2 to 10.2 J/cm^2) increase in the LIDT value was observed; however, at temperatures below −60 °C, the increase in LIDT stopped.

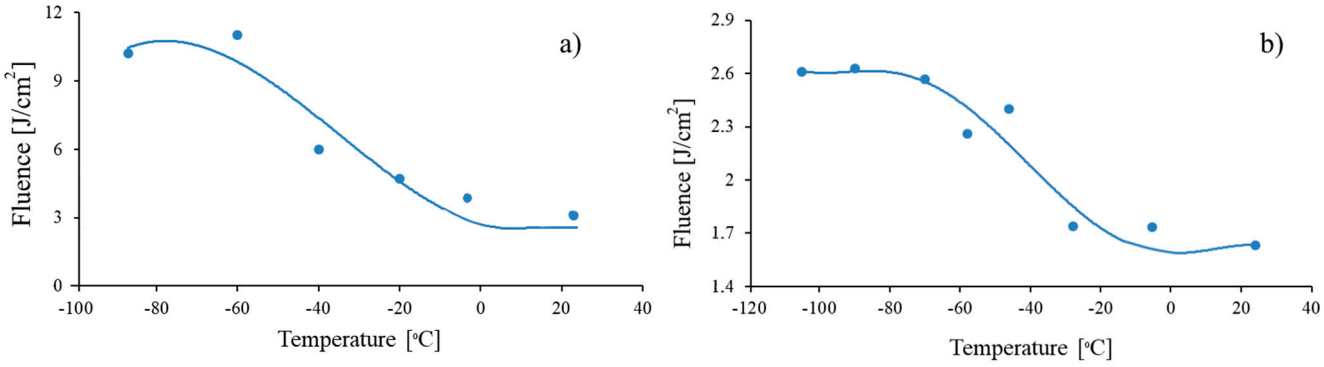

Figure 7. Dependence of the LIDT fluence W0d on the temperature of the ZGP crystal when exposed to Ho^{3+}:YAG laser radiation at a wavelength of 2091 nm with a laser beam diameter of 100 μm (**a**) and with a laser beam diameter of 270 μm (**b**) (adapted from [34]).

Measurements of the dependence of the LIDT on the crystal temperature were also performed with a laser beam diameter of 270 μm. The measurement results demonstrated a similar dependence of the LIDT on the crystal temperature (Figure 7b). In the temperature range from +24 to −106 °C, an increase in the LIDT value of more than 1.5 times (from 1.6 to 2.6 J/cm^2) was observed, and the increase in LIDT also stopped at temperatures below −60 °C.

It is known that ZGP is a high-ohm semiconductor with stable hole conductivity, the magnitude of which is difficult to change [57]. The typical temperature dependence of the concentration of free charge carriers in ZGP is described by an exponential curve with an activation energy of deep impurity centers of 0.3–0.6 eV. However, the obtained temperature dependence of the LIDT has a sigmoidal character and therefore cannot be

explained by the absorption of free carriers (holes), arising from the ionization of individual point defects as well as defects associated with edge dislocations.

The obtained temperature dependence of the LIDT was explained by the temperature dependence of the phonon occupation numbers, which participate together with optical quanta in indirect transitions of nonlinear absorption: valence band—impurity level [58]. In support of this assumption, it can be noted that with a decrease in the temperature of the crystal, the phonon occupation numbers increase, leading to a decrease in the probability of their participation in indirect transitions of electrons from the valence band to impurity levels [58,59].

5. Dynamic Processes in the ZGP Pre-Damage Region

Modern technologies allow for the use of a CCD camera to register the interference pattern of the reference and object waves. This process of recording holograms on a CCD camera and the subsequent numerical recovery of an image from them is called digital holography. Figure 7 shows the axial scheme of recording Gabor digital holograms. Light from a laser source (1) passes through a collimator (2), forming a beam of the required cross-section, then passes through the sample under study.

As a result, an interference pattern of the reference (part of the radiation that passes by the inclusions) and object (part of the radiation scattered by the inclusions) waves is formed. The camera registers this interference pattern and transfers it to the computer's memory. Subsequent mathematical processing by special computational algorithms [60] allows for the restoration of the spatial distribution in the investigated volume, namely the three-dimensional coordinates, sizes, shapes, and locations of each area of interest. Image restoration is numerical, with the image of the investigated volume being formed during processing layer by layer.

Since the Gabor scheme allows for reduced requirements for the spatial and temporal coherence of the light source [61], a semiconductor laser diode with a wavelength of 1.064 μm (position 1 in Figure 8) with an output power of 100 mW was used. A CCD camera with a matrix of 1600 × 1200 pixels, a pixel size of 7.4 μm × 7.4 μm, and physical dimensions of the matrix of 2/3 was used as the recording camera (position 4 in Figure 8). The long-wavelength boundary of the CCD camera's photosensitivity is limited to a wavelength of 1.1 μm. The spectral transparency ranges of the $ZnGeP_2$ compound, calculated for short wavelengths based on the bandgap width and for the long-wavelength edge based on the maximum three-phonon absorption, included the region from 0.64 to 9.0 μm, but the actual working spectral range with the coefficient of absorption not exceeding a value of 1 cm^{-1} was determined by wavelengths of 0.9 to 8.3 μm. Thus, for studies of $ZnGeP_2$ using digital holography on "transparency", sources that generate radiation in the spectral region near 1.06 μm and CCD matrices of the visible range can be used. These issues are discussed in detail in [62].

It is clear that the investigated area is limited by the camera aperture of ~ 11 mm. The holographic camera used to study the optical damage of the ZGP was designed for the creation of parametric converters of tunable radiation in the range of 3–8 μm, pumped by lasers emitting in a wavelength range of about 2 μm. The study of the LID was carried out using a scheme of digital hologram recording (Figure 8). Pulsed radiation from a Ho^{3+}:YAG laser with a PRR of ~10 kHz, pulse width of ~25 ns, and average power varying from 500 mW to 9 W, was focused by a short-focus lens L, onto the input face of a single ZGP crystal (manufactured by LOC). The use of a short-focus lens excluded the self-focusing of radiation in the volume of the investigated crystal. The exposure duration was ~30 s. Further, if optical damage was not observed, the laser radiation power was increased, and the irradiation process was repeated. The beam diameter at the front face of the single crystal was ~200 μm at the $1/e^2$ level. The side faces of the crystal were polished. The crystal was placed in a digital holographic camera, DGK 1.06, using holograms of the internal volume of the single crystal (in the direction perpendicular to the direction of the incident radiation) which were recorded with a frame rate of ~7 Hz.

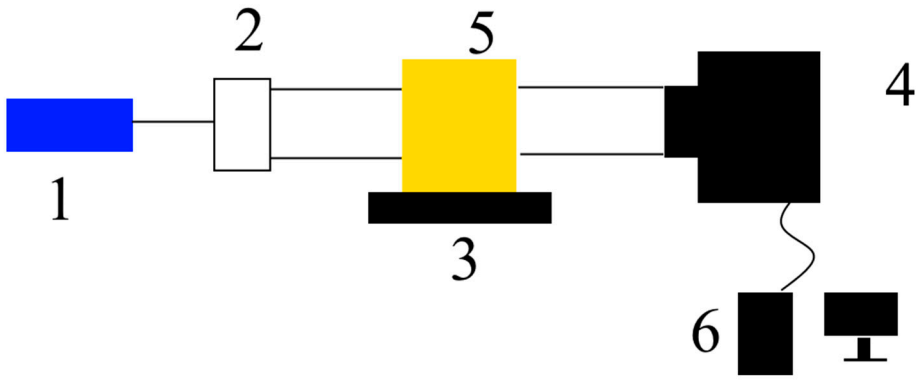

Figure 8. Axial scheme for recording digital holograms: 1—laser emitter, 2—collimator, 3—two-coordinate positioner, 4—CCD camera, 5—studied sample, and 6—computer.

The setup of testing the ZGP LID with the digital holographic technique is shown in details in Figure 9. Figure 10 shows the reconstructed images obtained in the study. Figure 10a shows the reconstructed image of the plane of the best installation of the area of the single crystal where the breakdown develops, before the formation of the damaged track and the formation of the glowing area; the red arrow shows the direction of the radiation incidence. Figure 10b is the splicing of frames of the reconstructed image of the plane of the best installation, on which the process of the development of the optical damage and the spread of the glowing area (the glowing "ball") in the single crystal was recorded with reference to the length of the crystal and time; the red arrow shows the direction of the radiation incidence, the yellow arrow shows the direction of the movement of the area in which the optical damage was formed. Figure 10c is the reconstructed image of the plane of the best installation of the area of the single crystal with a characteristic damage track above the LIDT.

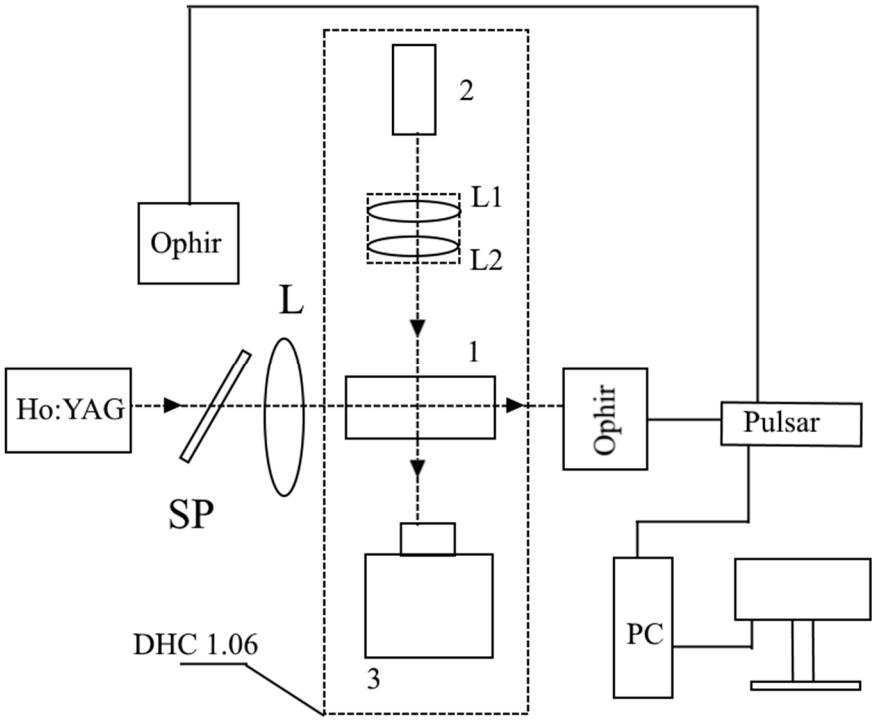

Figure 9. Diagram of the beam loading stand for studying the ZGP LID by the digital holographic technique: Ho^{3+}:YAG laser, SP is a dividing plate, Ophir is the power meter from Ophir company, synchronization is a device synchronization unit, DHC 1.06 is the digital holographic camera, PC is a personal computer, 1 is the ZGP single crystal, 2 is the laser module ML 150-1053-100-TTL, L is the short-focus lens, and 3 is the matrix photodetector (adapted from [62]).

The impact of the Ho^{3+}:YAG laser pulses on the ZGP crystal caused the appearance of a luminous spot with a diameter of 0.7–1 mm on the output optical surface, and its subsequent movement in the crystal towards the input optical surface, i.e., in the direction opposite to the propagation of the Ho^{3+}:YAG laser radiation (Figure 10b). The resulting luminous spot can be associated with luminescence arising from the recombination of non-equilibrium carriers through the levels of point defects [32]. The movement of the luminescent "cloud" is accompanied by the formation of an optical damage channel (track) with a diameter of 70–75 µm. The dynamics of the development of optical damage at an average laser fluence of 0.3 J/cm^2, which was obtained by splicing frames reconstructed from a series of holograms obtained with an interval of ~143 ms, is shown in Figure 10b. The frames are separated from each other by black lines; each frame corresponds to the path traveled by the luminous spot that is fixed when the damage track is formed inside the crystal.

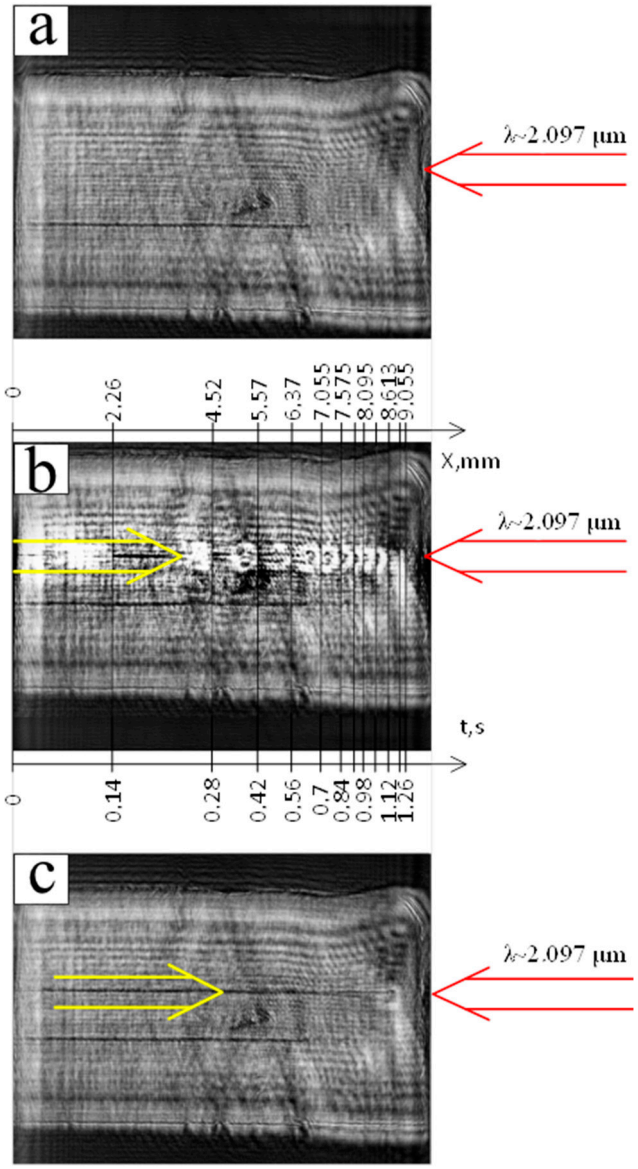

Figure 10. Results of digital hologram processing during the optical damage of a ZGP single crystal by laser irradiation: before LID (**a**), during LID (**b**), and after LID (**c**). The red arrows show the direction of the Ho^{3+}:YAG beam propagation, the yellow arrows show the propagation direction of the glowing ball (adapted from [32]).

The position of the luminous spot relative to the exit crystal face, X, was determined at the time, *t*, relative to the LID start (Figure 11).

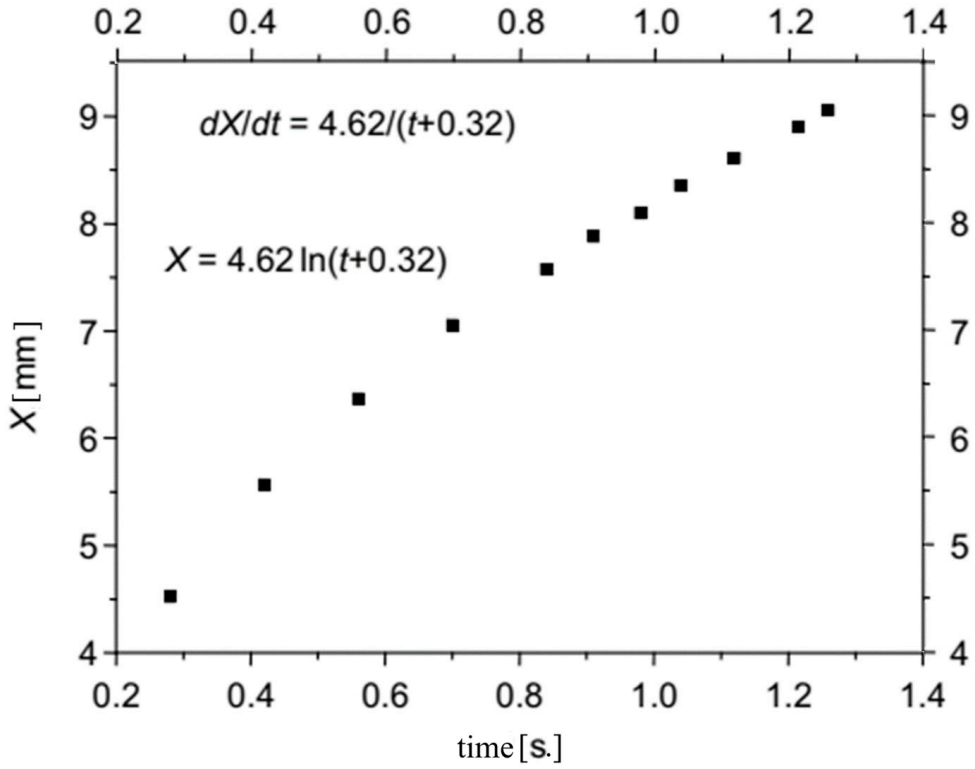

Figure 11. Dependence of the optical damage track location X (the luminous spot position) on time t at a laser pulse fluence of 0.3 J/cm^2, diameter of the Ho^{3+}:YAG laser beam on the entrance face of the single crystal of ~200 μm (at the 1/e^2 level), PRR of ~10 kHz, and the pulse width of ~25 ns (adapted from [32]).

The full duration of the optical damage formation in a 10 mm ZGP crystal was determined as ~1.3 s. The instantaneous speed of movement of the luminous spot—V (mm/s) = dX/dt—in the initial period, as it turned out, was significantly higher than the speed of its advancement in the second half of the crystal. So, if the first 4.5 mm were damaged with a speed of V_{in}= 4.52/0.28 ≈ 16 mm/s, then, at the final stage of the damage, the speed of track formation was V_{fin} = (9.055–8.095)/0.14 ≈ 3 mm/s. The damage stopped at the destruction of the entrance face of the crystal with a conical damaged track formation.

Using the available experimental data and the ORIGIN LAB mathematical software, a logarithmic dependence of the track length on the time of exposure was obtained (see Figure 11). The dependence of the speed of propagation of the luminous spot in a ZGP crystal at a beam fluence of 0.3 J/cm^2 obtained by the least squares method is a smooth monotonic function of the current time:

$$V(mm/s) = dx/dt = 4.62/(t + 0.32), \quad (1)$$

where *t* is the time in seconds relative to the LID initial moment (when the glowing spot appeared).

According to the given approximation, the speeds of the spot propagation (the damage track formation) were determined as V_{in} = 14.4 mm/s at the initial stage, and V_{fin} = 3.5 mm/s at the final stage of the LID. The slowing down of the track formation process was not consistent with the impact ionization model with a power law dependence on the avalanche generation of electron-hole plasma. At the same time, positive feedback between the temperature increase and the ZGP absorption coefficient increase can be an alternative to impact ionization and can provide a high concentration of non-equilibrium

carriers due to a sharp temperature jump during the absorption of pumping radiation in the crystal volume. Then, the time delay at the beginning of track formation can be attributed to the time spent on heating the crystal volume to a high temperature by laser radiation.

The generation of carriers by increasing temperature does not create non-equilibrium carriers capable of recombination accompanied by luminescence. Therefore, in order to explain the appearance of a luminous area in the crystal excited by an intense laser beam, it was necessary to take into account dimensional factors, namely, the ratio of the diameters of the laser beam (200 μm) and the luminescent "cloud", the brightest glow of which was recorded at a distance of 250–400 μm (Figure 10b) from the forming "dark" LID track.

The change in the crystal structure under laser irradiation indicated an increase in the instantaneous effective temperature to values that exceed the melting point of the ZGP compound −1025 °C [32,63]. A lower-temperature phase transition $ZnGeP_2$(sph)→$ZnGeP_2$ (halc) near 950 °C can be excluded from consideration since it was observed only at low temperatures and was associated with the ordering of atoms in the cation sublattice.

A sharp increase in the temperature of the crystal and its local melting led to subsequent solidification of the melt, forming an LID track along the laser beam and the diffusion of free carriers from the heated area of the crystal in the direction perpendicular to the laser beam. The transverse temperature gradient perpendicular to the direction of the propagation of laser radiation causes free carriers to diffuse from the high-temperature generation zone (in which they are in equilibrium and cannot be manifested in luminescence) to the unheated regions of the crystal; there, they are in non-equilibrium and recombine, at least partially, at the luminescence transitions (levels of point defects), creating a toroidal distribution of the intensity of luminescence.

In order to explain the decrease in the speed of formation of the damage tracks from the coordinate (from the time), in [32], it was assumed that the conical form of the track was responsible, i.e., due to the volume of the material heated by the laser beam. As it turned out, (see Figure 12), the diameter of the conical track increased from ≈40 μm at the initial section of the track (at the crystal exit) to ≈100 μm at the entrance aperture of the crystal. Accordingly, the cross-section changes by approximately 3–4 times, which is close to the ratio of the track formation speeds on the input and output surfaces of the crystal. However, in addition to the pronounced tendency for the track diameter to increase with the coordinate, there were quasi-periodic variations in the diameter of the LID tracks with maxima at ≈3 mm, 5 mm, and 7 mm, which were compared with areas near the intersection points of the optical damage track with "dark" growth bands, i.e., in places with an increased absorption coefficient relative to the average value.

Figure 13 shows the LID in another point of the same crystal under more powerful laser irradiation—with a fluence of 0.6 J/cm^2. In this case, optical damage also occurred near the exit surface, but the track formation process proceeded two times (and significantly) faster, which, in principle, agrees with the twofold increase in the beam fluence and the thermal origin of the LID. Processing of the holographic data showed that the duration of the damage-track formation was ~0.67 s.

In the photographs in Figure 13e,f, the reconstructed images of the crystal before laser exposure and at the moment when the glowing (luminescent) spot reached the front surface of the crystal are shown. By comparing the geometric (dimensional) parameters of the images, it was found that at the final stage of optical damage, when the formation of the track is completed, the length of the crystal in the longitudinal direction at the point of exit of the track to the surface increased by ~dL = 117 μm (Figure 13f), and in the transverse direction it decreased by ~ 103 μm (Figure 13e).

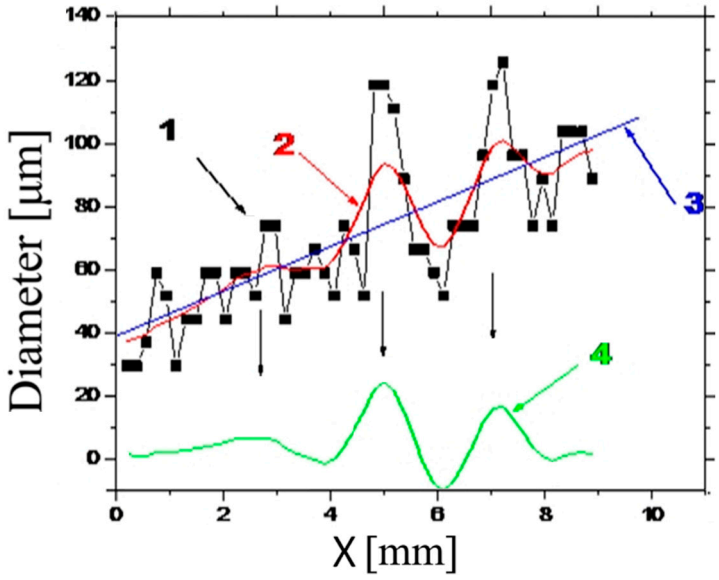

Figure 12. Dependence of the diameter D, μm, of the LID track on the distance X, mm, measured from the exit surface towards the incident laser beam. Curve 1 includes the data obtained from measurements; curve 2 represents the data after double smoothing by five points; line 3 is the linear regression; and curve 4 is the deviation of the smoothed values from the regression line (adapted from [32]).

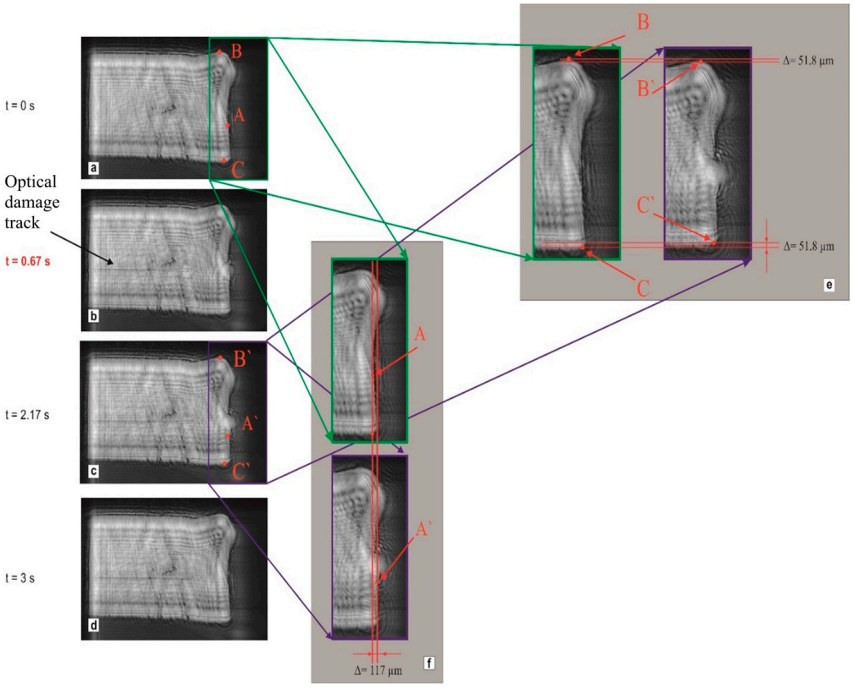

Figure 13. Results of the processing of digital holograms during the optical damage of a single ZGP crystal by laser radiation with a fluence of 0.6 J/cm^2: single crystal before radiation exposure (**a**); material breakdown (**b**); thermal expansion of the crystal near the location of the optical damage track (**c**); relaxation of the dimensions of the single crystal after exposure to radiation (**d**); transverse deformation of the surface at the moment of optical damage relative to the element surface in the absence of laser radiation (**e**); and longitudinal deformation in the reconstructed image of the element at the LID moment relative to the element in the absence of laser radiation (**f**). The indicating points on the crystal surface are numbered as A, B, C before the LID deformation, and A', B', C' after the LID deformation (adapted from [32]).

A rough estimate of the temperature developing in the central part of the damage track can be made based on the relative longitudinal deformation of the crystal dL/L ≈ 0.0117 and the coefficients of thermal expansion (β_{av}) of ZGP [32,63]. At a temperature of >573 K the coefficient of thermal expansion has a value of $\beta_{av}(>573\ \mathrm{K}) = 8.59 \cdot 10^{-6}\ \mathrm{K}^{-1}$. The temperature required for the elongation of the crystal by 117 μm can be estimated by $T\frac{=\left(\frac{dL}{L}\right)}{\beta_{av}} = 1362^0$ K. Therefore, according to the estimation, to change the length of the crystal by 117 μm, it will be necessary to increase its temperature to $T_{TP} = 1362^0$ K. The obtained value of the temperature in the damage track is higher than the melting point of the compound by approximately ≈ 60 K and, in principle, agrees with the conclusion about the thermal origin of the LID track.

At the used levels of laser beam intensity, in contrast to the degradation of the optical properties in the damaged region, the mechanical deformation of the crystal was elastic, and, after the completion of the damage track formation process, a rapid lattice relaxation occurred along the entire length of the crystal.

As a result of comparative studies of the crystal before, during, and after LID, it was established that the propagation channel of laser radiation darkens in the pre-damage region of the laser parameters. Visually, this effect manifested itself in the reconstructed images of the plane of the best setup in the form of the darkening of the area of the crystal in which the laser radiation was propagated (Figure 14). This process is clearly demonstrated in Figure 14b: a dark track is formed in the channel of propagation of an intense laser beam (for test radiation at a wavelength of 1064 nm). The darkening was reversible: when the density of the incident radiation decreased below a certain level or when the laser exposure to the crystal was completely stopped, the area of darkening disappeared—Figure 14c. The relaxation time of the area of darkening of the laser channel was less than 5 ms.

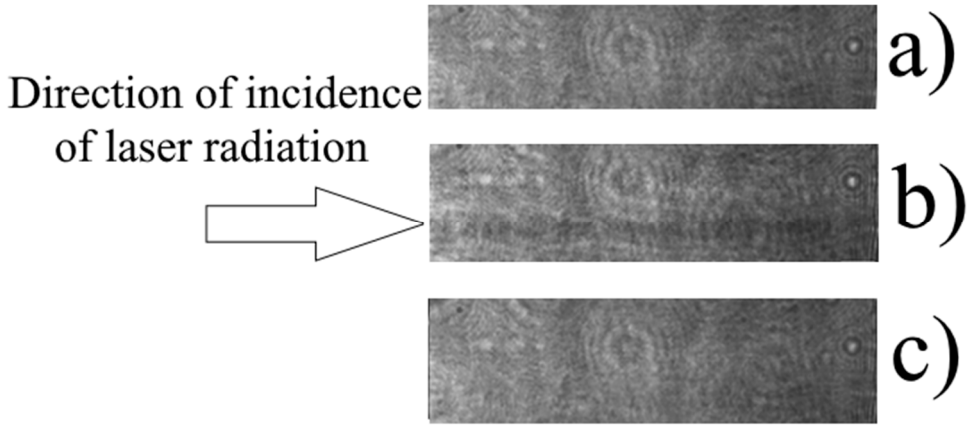

Figure 14. Reconstructed image of the hologram of the volume of the single ZGP crystal before the test (**a**), under the influence of the pulsed radiation of the Ho^{3+}:YAG laser at LIDT fluence (**b**), and 10 ms after the cessation of the action of the Ho^{3+}:YAG laser radiation (**c**) (adapted from [34]).

The darkening of the channel of propagation of a powerful laser beam in the pre-damage region can be explained by a local decrease in the band gap width of the ZGP crystal upon heating. Indeed, it is known that the band gap width of semiconductors decreases with increasing temperature [34]. This leads to an increase in the absorption of the testing beam at 1064 nm.

Importantly, in most of the tests performed with ZGP elements of different lengths and manufactured with different technological growing and post-growing procedures (in more than 90% of the total number of measurements), the LID began at the exit surface of the sample. The LIDT difference on the exit and entrance surfaces can be explained by the different intensities (and the fluence) of the laser beam at the surfaces. The last difference could be caused by two effects: thermal self-focusing (the thermal lens formation) in the ZGP crystal [64], and a difference in the maximum electric field amplitude of the

optical waves at the surfaces due to the phase difference of the waves reflected from the boundaries [65]. The thermal self-focusing may be an impotent effect for long samples or the ZGP-tandem OPOs [66] when the focal length is comparable with the element length. The second effect of the interference between the incident and reflected waves at the surfaces of a sample (depending on the boundary phase changes) appears to be more reasonable for a thin element with low absorption [67]. Indeed, the basic fact is that the field of the Fresnel reflected wave at the entrance surface is 180° out of phase with the incident wave field, whereas, at the exit surface, the reflected wave field is in phase with the incident wave field. Thus, the net electric field is higher at the exit surface than at the entrance surface for a given input irradiance. The ratio of the exit to entrance wave intensities I_{ex} and I_{ent}, respectively, can be estimated (on the crystal boundaries without any AR coating and higher order reflections) by the following expression [65]:

$$I_{ex}/I_{ent} \approx 4n^2/(n+1)^2 \times \exp(-\alpha L), \quad (2)$$

where n is the refractive index, α is the absorption coefficient, and L is the sample length. The estimation of the intensity ratio by Expression (2) for a ZGP crystal with a refractive index of ~3.15 (at 2.1 μm [68]) yields 2.3 × exp (-αL). This value is more than 1 for $\alpha L < 0.83$. Therefore, the scenario with the LID initiation near the exit surface due to the higher intensity of the exit beam appears to be quite natural even for a long ZPG sample with a length L = 3 cm and an absorption coefficient $\alpha < 0.28$ cm^{-1} (the ZGP samples used had a much lower absorption coefficient).

6. Effect of Pre-Damage Phenomena on ZGP OPO Operation

A transparent nonlinear ZGP crystal (produced by LOC) with linear dimensions of 20 × 6 × 6 mm^3 cut at angles θ ≈ 54.5° and φ ≈ 0° was used to examine the effect of the pre-damage phenomena on ZGP OPO operation [69]. The absorption of radiation at a wavelength of 2.097 μm of the sample was 0.029 cm^{-1}.

The scheme of the experimental setup is shown in Figure 15. A periodically pulsed Ho^{3+}:YAG laser was used as a pump source for the OPO. Optical isolation between the OPO cavity and the Ho^{3+}:YAG laser cavity was provided by an optical isolator (OI).

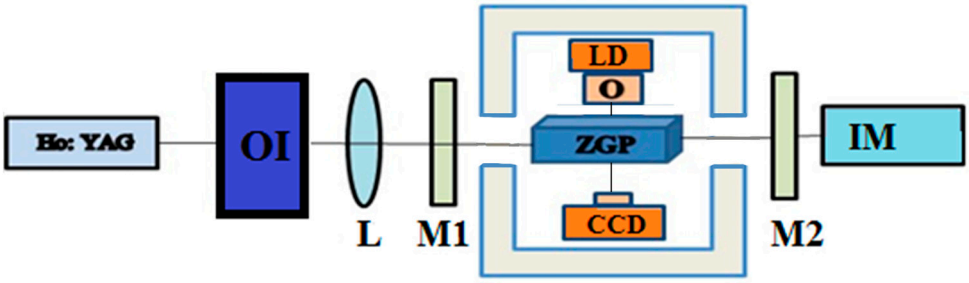

Figure 15. Scheme of the ZGP OPO setup with Ho^{3+}:YAG laser pumping: Ho^{3+}:YAG laser, OI is the optical isolator, L is the lens, M1 is the input mirror of the OPO cavity, M2 is the output mirror of the OPO cavity, ZGP is the single crystal, LD is the laser diode, O is an objective, and IM is a power meter (adapted from [69]).

The Ho^{3+}:YAG laser used for the experiments had the following energy characteristics: the maximum average power of radiation in pulsed mode was 15 W, the PRR was 10 kHz, and the pulse width at half-height was 26 ns. The OPO cavity was formed by a plane mirror M1 with transmission of ~99% at the pump wavelength and reflection of ~99% at the generated wavelength. The plane mirror M2 had a transparent coating with a transmission of ~99% at the pump wavelength with a beam-splitter coating with 50% reflection at the generation wavelength, which made it possible to implement single-pass pumping. The ZGP crystal with AR coating, applied to the working surfaces at wavelengths of λ = 2.097 μm and λ = 3.5–5 μm, was placed in the cavity formed by mirrors M1 and

M2. The side faces of the ZGP element were also polished. Through the side polished surfaces of the ZGP element, a hologram of the internal volume of the crystal (in the direction perpendicular to the direction of the incident radiation) was recorded using a digital holographic camera.

The results obtained from measuring the energy characteristics of the ZGP OPO with Ho^{3+}:YAG laser pumping are presented in Figures 16–18. Figure 16 shows the dependence of the average power of radiation generated in the OPO and the generation efficiency on the PRR pumping.

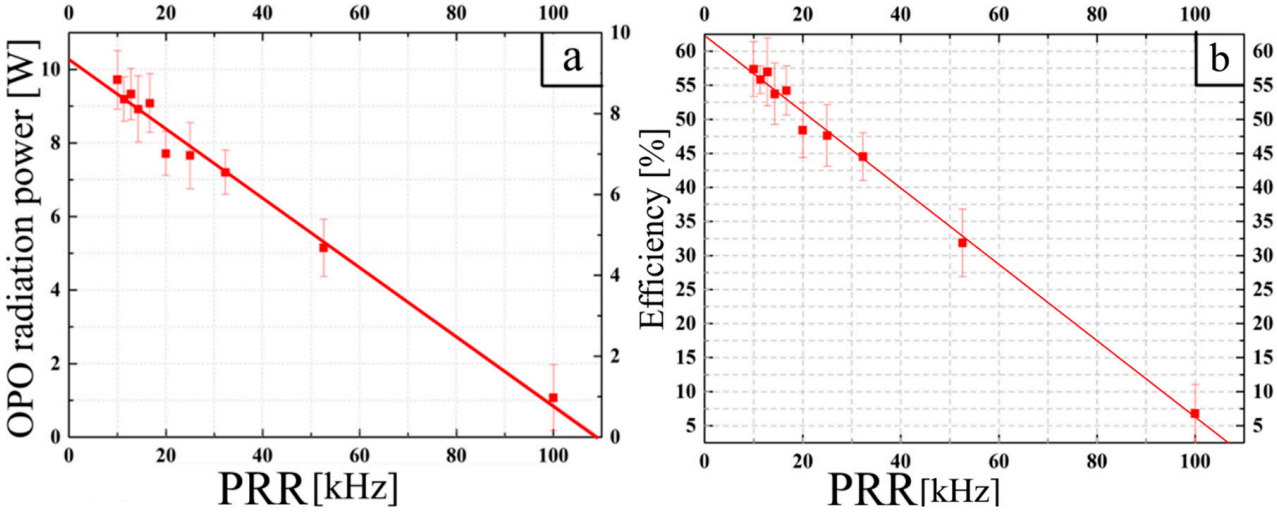

Figure 16. Dependence of the average power of the generated radiation on the PRR pumping at an average power of 16.3 W (**a**). Dependence of the efficiency of parametric generation on the PRR pumping at an average power of 16.3 W (**b**) (adapted from [69]).

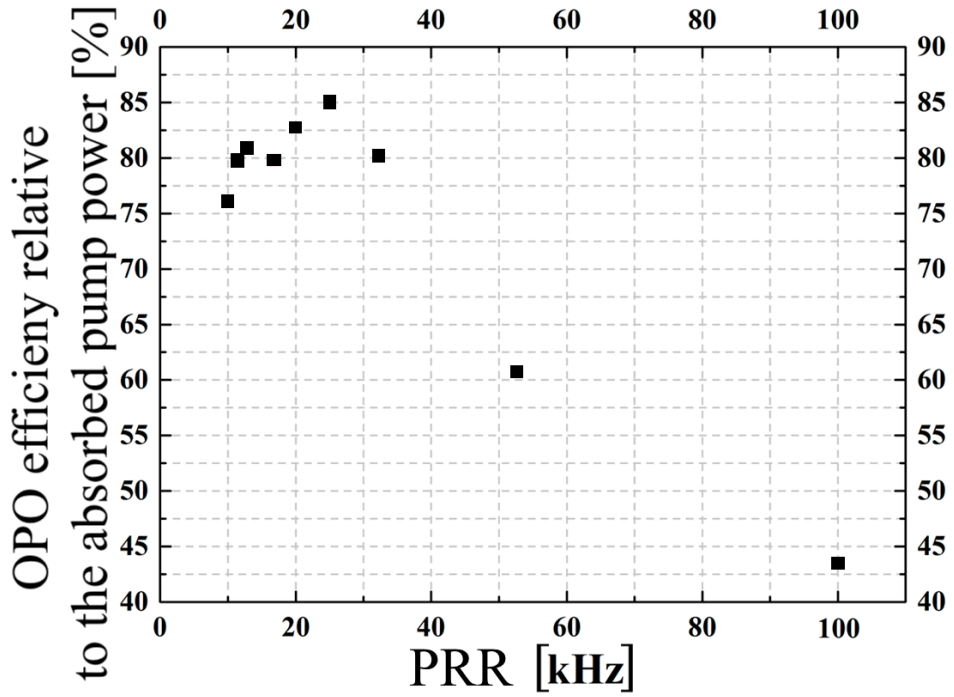

Figure 17. Dependence of the OPO efficiency relative to the absorbed pump power on the pumping PRR (adapted from [69]).

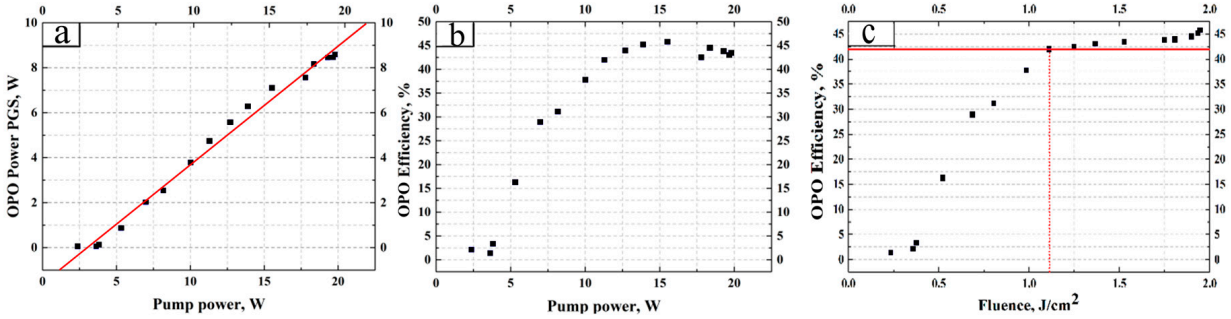

Figure 18. The output OPO power and efficiency vs. the incident pump power (**a**); the OPO efficiency vs. the incident pump power (Po) (**b**), and the OPO efficiency on the pump fluence (**c**) (adapted from [69]).

During the measurements, the average pump power of 2.097 μm remained constant at 16.3 W, while the PRR varied from 10 to 100 kHz. It is worth noting that stable generation in the Ho^{3+}:YAG laser was observed up to 50 kHz PRR; at a PRR of 100 kHz, the laser operation was unstable. The maximum value of the OPO efficiency achieved in the experiment was 57.35% (Figure 16b). The maximum value of the OPO average power was 9.72 W at a PRR of 10 kHz (Figure 16a).

Using the available experimental data and ORIGIN LAB mathematical software, the dependence of the efficiency of the pump power absorbed in the crystal (without taking into account the part of the pump power that escaped from the cavity) on the pumping PRR was obtained. The maximum value of the efficiency of the absorbed power was ~85% (Figure 17).

Further studies were conducted on the energy characteristics dependent on the pump power at a PRR of 10 kHz. The maximum value of the OPO output power obtained in the experiment was 8.46 W (Figure 18).

The maximum efficiency was ~45.74%. From Figure 18 c, it is clear that when the pump power reached ~11 W and the energy density reached ~1.2 J/cm^2, the efficiency stopped growing and reached a saturation point.

Studies were then conducted on the dependence of the transmission of the nonlinear crystal on the power of the test radiation and the energy density of the radiation falling on the crystal. The results obtained (Figure 19) are presented in the form of dependencies of the transmission on the pump power and the transmission on the energy density of the radiation falling on the crystal; the PRR varied from 10 kHz to 30 kHz with a step of 10 kHz.

Figure 20 shows the restored holograms. At a power of up to 0.7 J/cm^2, the holographic camera did not detect any changes. With an increase in the pump fluence from 0.7 to 0.9 J/cm^2, the formation of a dark area along the entire length of the crystal was observed. With an increase in the fluence to 1.2 J/cm^2, this area became darker. At a power of more than 1.2 J/cm^2, a damaged track inside the ZGP element was registered.

An analysis of the dependencies presented in Figures 16–19 and the dark tract images in Figure 20 allows us to conclude that the ZGP transmission decreased near the LIDT (above the pump fluence of 1 J/cm^2). With a decrease in PRR at the same average power (and an increase in the pumping pulse fluence), this dependence became more pronounced. These dependencies can be explained by an induced nonlinear absorption near the LIDT (below the LIDT), which increased with the growth of the pumping pulse fluence. Nonlinear absorption can additionally contribute to the ZDP optical damage.

Further studies, which were carried out with a pumping fluence of 0.9 J/cm^2 (which was two times less than the ZGP LIDT), registered a stable OPO operation for more than 6 min (this operation time was limited only by the thermal management of the system). If the pump fluence was more than 1.3 J/cm^2, when the darkening was observed, the OPO operation time was limited by the LID that occurred after 30 s.

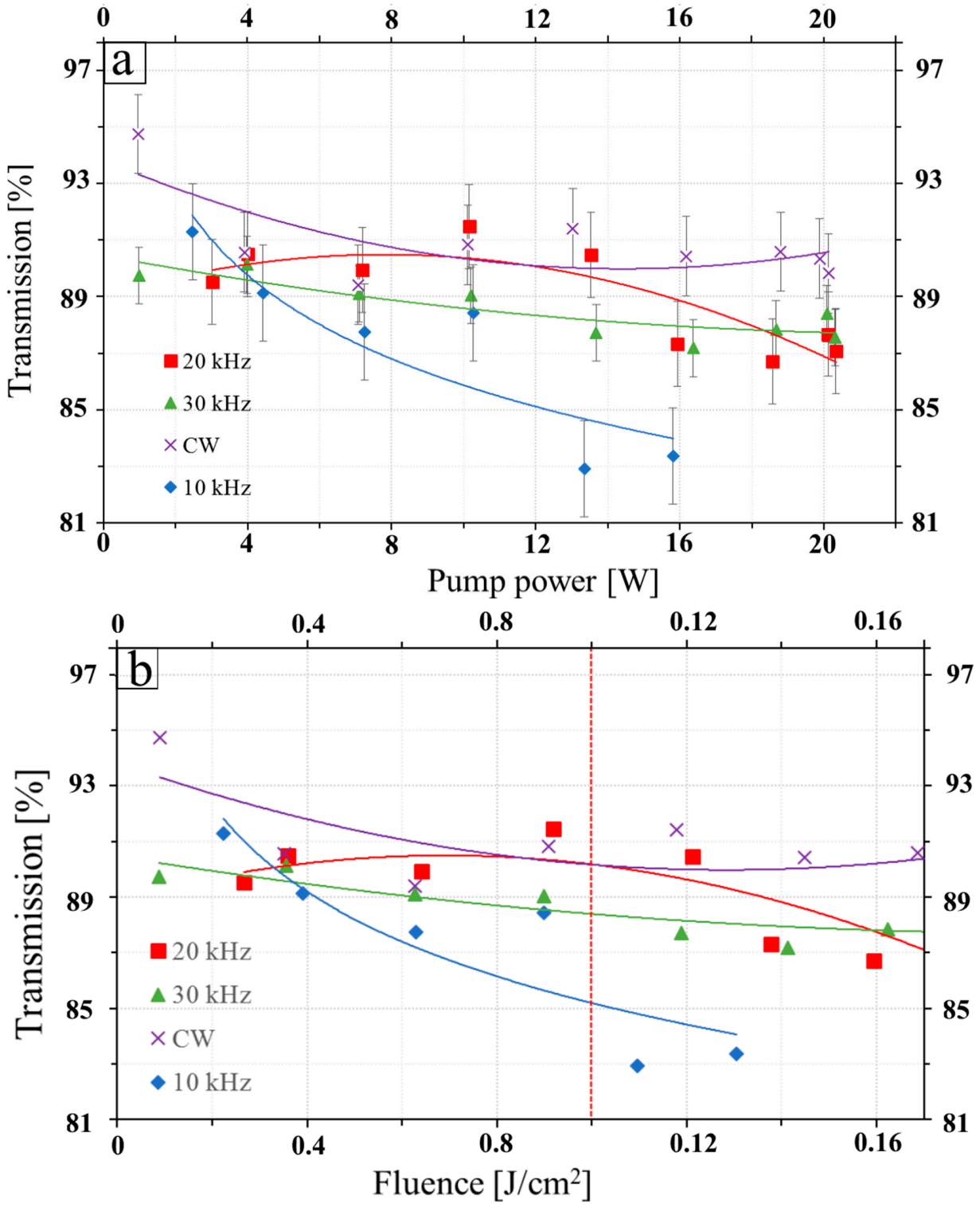

Figure 19. Dependence of the transmission on the incident pump power (**a**) and dependence of the transmission on the pump fluence (**b**). The different color lines indicate the corresponding PRR (adapted from [69]).

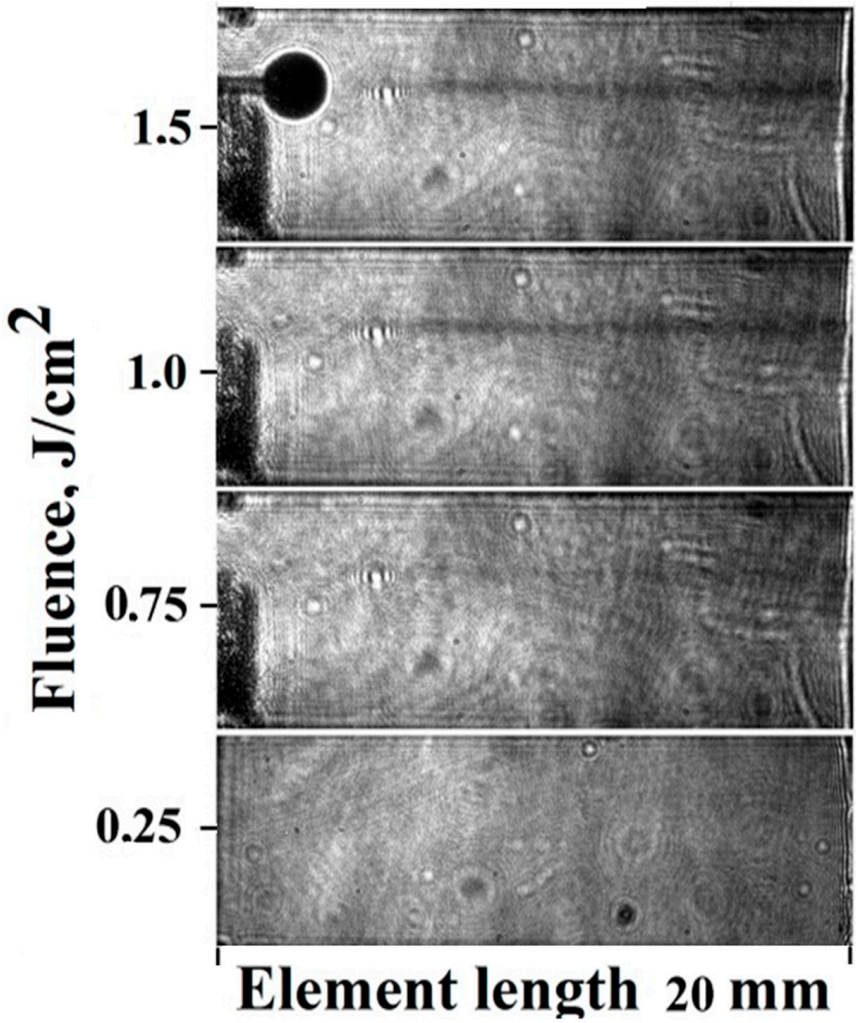

Figure 20. Restored image of the ZGP crystal taken with a holographic camera when laser radiation of different powers was applied to the nonlinear optical crystal ZGP (adapted from [69]).

7. Conclusions

The paper presents up-to-date information on the initiation of LID inside single ZGP crystals under 2 μm Ho^{3+}:YAG nanosecond laser irradiation and methodology for increasing the ZGP crystal's LIDT. The main findings are as follows:

(1) It has been shown that an order of magnitude reduction in the number of bulk defects and dislocation concentration inside ZGP crystals increased the LIDT by more than three times.

(2) It has been shown that the diffusion doping of single ZGP crystals with Mg and Se leads to a higher LIDT. After annealing at 750 °C, the destruction threshold of samples doped with Mg and Se increased by 31% and 21%, from 2.2 ± 0.1 J/cm^2 to 2.9 ± 0.1 and 2.7 ± 0.1 J/cm^2, respectively. The opposite trend was observed when ZGP was doped with Ca. A correlation was observed between the optical breakdown threshold and the electro-physical parameters of crystals after doping, in particular, when it comes to the conductivity of samples. A decrease in conductivity was observed when the ZGP samples were doped with Mg and Se, while the conductivity of ZGP increased after doping with Ca compared to an undoped annealed sample. Studies have shown that there is a technological possibility to increase the LIDT of ZGP crystals by reducing the conductivity of samples using controlled doping.

(3) An increase in the LIDT was found after applying an AR coating. In the case of a coating based on ZnS and Al_2O_3 materials, the LIDT increased by 55% compared to

an uncoated sample. It was assumed that there were no local composition fluctuations or mechanical stress in the layers of the transparent coating, which in turn led to good adhesion of the multilayer coating to the polished surface of the crystal and increased the LIDT compared to the uncoated sample by closing the broken chemical bonds and bulk defects that came out on the polished surface.

(4) Data were obtained on the dependence of the LIDT fluence on the laser beam diameter and intensity, the PRR, and the exposure.

(5) A strong dependence of LIDT at 2.1 μm on the crystal temperature was found. The observed sharp increase in the threshold energy density (up to three times the initial value) when the ZGP temperature was reduced from 0 °C to −60 °C can be explained by the temperature dependence of the filling number of phonons. The increase in the filling number of phonons, with a decrease in the temperature of the crystal, leads to a decrease in the probability of their participation in indirect electron transitions from the valence band to impurity levels, and, accordingly, to a decrease in the nonlinear absorption of the crystal.

(6) Visualization of the optical damage dynamics using digital holography showed the formation of an optical pre-damage track along the laser beam. The process of the solidification of the molten material leads to the diffusion of free charge carriers from the heated region of the crystal in the direction perpendicular to the laser beam. The effect above the LIDT is accompanied by the appearance of a luminous spot near the exit optical surface inside the crystal and the subsequent movement of this luminous spot towards the input optical surface, i.e., in the direction opposite to the propagation of laser radiation. This luminous spot can be explained by the recombination of the formed non-equilibrium charge carriers.

(7) Using a digital holographic camera, it was found that a pulsed beam intensity greater than or equal to the LIDT of the crystal leads to elastic deformations of the crystal in the longitudinal direction at the moment of formation of the damage track. These deformations were attributed to the thermal expansion of material in the damage track area, caused by a sharp increase in the local temperature along the laser beam, to values exceeding the melting temperature of the crystal.

(8) The presence of the reversible "photo darkening" area along the propagation path of a powerful laser beam at 2.1 μm in ZGP crystals below the LIDT was established. Such reversible photodarkening of the propagation channel can be explained by the local decrease in the band gap width of ZGP crystal due to heating.

(9) Over the course of studying the energy characteristics of the OPO based on a ZGP crystal and using the results of the visualization of the processes taking place inside the crystal, we established that when the pump intensity reaches half the LIDT threshold, the OPO efficiency stops growing and the darkening of the beam path inside the crystal starts forming. These effects were accompanied by a decrease in transmission when the crystal was irradiated outside the resonator, which may indicate significant nonlinear absorption. The results indicate that these processes are interrelated. Nonlinear absorption may be the cause of the decrease in the efficiency of parametric conversion and may be a factor that initiates optical damage.

(10) This review shows the significant potential for increasing the LIDT of ZGP crystals by improving the structural perfection of the crystal and improving the quality of the crystal surfaces by improving the technology of crystal growth, post-growth processing, polishing, and the AR coating of working surfaces.

Author Contributions: Conceptualization, N.Y.N.Y. and O.A.; methodology, N.Y.N.Y., V.D. and A.G.; software, M.Z., S.P. and V.K.; validation, E.S., I.O.K. and A.K. (Andrey Khudoley); formal analysis, V.K.; investigation, A.L., A.K. (Andrey Kalsin) and I.E.; resources, O.A.; data curation, H.B.; writing—original draft preparation, H.B.; writing—review and editing, N.Y.N.Y.; visualization, E.S.; supervision, V.D.; project administration, O.A.; funding acquisition, O.A. All authors have read and agreed to the published version of the manuscript.

Funding: This research was supported by the Russian Science Foundation (project No. 22-12-20035, https://rscf.ru/en/project/22-12-20035, accessed on 25 March 2022) and the Ministry of Education, Science and Youth Policy of the Nizhny Novgorod Region (agreement No. 316-06-16-17/22 accessed on 31 March 2022).

Institutional Review Board Statement: Not applicable.

Informed Consent Statement: Not applicable.

Data Availability Statement: Not applicable.

Conflicts of Interest: The authors declare no conflict of interest. The funders had no role in the design of the study; in the collection, analyses, or interpretation of data; in the writing of the manuscript, or in the decision to publish the results.

References

1. Yulong, S.; Meng, J.; Wei, T.; Xie, Z.; Jia, S.; Tian, W.; Zhu, J.; Wang, W. 150 Gbps multi-wavelength FSO transmission with 25-GHz ITU-T grid in the mid-infrared region. *Optics Express* **2023**, *31*, 15156–15169.
2. Yevtushenko, A.; Rozniakowska-Klosinska, M. *Encyclopedia of Thermal Stresses, Laser-Induced Thermal Splitting in Homogeneous Body with Coating*; Springer: Berlin, Germany, 2014.
3. Parfenov, V.A. *Laser Materials Microprocessing*; Saint Petersburg Electrotechnical University "LETI": Saint-Petersburg, Russia, 2011; pp. 5–11.
4. Edwards, G.; Logan, R.; Copeland, M.; Reinisch, L.; Davidson, J.; Johnson, B.; Maciunas, R.; Mendenhall, M.; Ossoff, R.; Tribble, J.; et al. Tissue ablation by a free-electron laser tuned to the amide II band. *Nature* **1994**, *371*, 416–419. [CrossRef] [PubMed]
5. Mackanos, M.A.; Simanovskii, D.; Joos, K.M.; Schwettman, H.A.; Jansen, E.D. Mid infrared optical parametric oscillator (OPO) as a viable alternative to tissue ablation with the free electron laser (FEL). *Lasers Surg. Med.* **2007**, *39*, 230–236. [CrossRef] [PubMed]
6. Soldatov, A.N.; Vasilyeva, A.V.; Polunin, Y.P.; Kuksgauzen, D.A.; Kostyrya, I.D. Strontium vapor generator-amplifier system for bone ablation. *Bio-Technosphere* **2012**, *3*, 47.
7. Kozub, J.; Ivanov, B.; Jayasinghe, A.; Prasad, R.; Shen, J.; Klosner, M.; Heller, D.; Mendenhall, M.; Piston, D.W.; Joos, K.; et al. Raman-shifted alexandrite laser for soft tissue ablation in the 6- to 7-μm wavelength range. *Biomed. Opt. Express* **2011**, *2*, 1275–1281. [CrossRef] [PubMed]
8. Serebryakov, V.S.; Boĭko, E.V.; Kalintsev, A.G.; Kornev, A.F.; Narivonchik, A.S.; Pavlova, A.L. Mid-IR laser for high-precision surgery. *J. Opt. Technol.* **2015**, *82*, 781–788. [CrossRef]
9. Ze, L.; Shen, Y.; Zong, N.; Bian, Q.; Wang, E.; Chang, J.; Bo, Y.; Cui, D.; Peng, Q. 1.53 W all-solid-state nanosecond pulsed mid-infrared laser at 6.45 μm. *Opt. Lett.* **2022**, *47*, 1359–1362.
10. Todd, M.W.; Provencal, R.A.; Owano, T.G.; Paldus, B.A.; Kachanov, A.; Vodopyanov, K.L.; Hunter, M.; Coy, S.L.; Steinfeld, J.I.; Arnold, J.T. Application of mid-infrared cavity-ringdown spectroscopy to trace explosives vapor detection using a broadly tunable (6–8 μm) optical parametric oscillator. *Appl. Phys. B* **2002**, *75*, 367–376. [CrossRef]
11. Bobrovnikov, S.M.; Matvienko, G.G.; Romanovsky, O.A.; Serikov, I.B.; Sukhanov, A.Y. *Lidar Spectroscopic Gas Analysis of the Atmosphere*; IOA SB RAS: Tomsk, Russia, 2014; p. 510.
12. Romanovskii, O.A.; Sadovnikov, S.A.; Kharchenko, O.V.; Yakovlev, S.V. Development of Near/Mid IR differential absorption OPO lidar system for sensing of atmospheric gases. *Opt. Laser Technol.* **2019**, *116*, 43–47. [CrossRef]
13. Bochkovskii, D.A.; Vasil'eva, A.V.; Matvienko, G.; Yakovlev, S.V. Application of a strontium vapor laser to laser remote sounding of atmospheric composition. *Atmos. Ocean. Opt.* **2012**, *25*, 166–170. [CrossRef]
14. Schunemann, P.G.; Zawilski, K.T.; Pomeranz, L.A.; Creeden, D.J.; Budni, P.A. Advances in nonlinear optical crystals for mid-infrared coherent sources. *J. Opt. Soc. Am. B* **2016**, *33*, D36–D43. [CrossRef]
15. Vodopyanov, K.L.; Laseryanov, K.L. *Infrared Sources and Applications*; John Wiley & Sons Inc.: Hoboken, NJ, USA, 2020.
16. Das, S. Optical parametric oscillator: Status of tunable radiation in mid-IR to IR spectral range based on $ZnGeP_2$ crystal pumped by solid state lasers. *Opt. Quantum Electron.* **2019**, *51*, 70. [CrossRef]
17. Hemming, A.; Richards, J.; Davidson, A.A.; Carmody, N.; Bennetts, S.; Simakov, N.; Haub, J. 99 W mid-IR operation of a ZGP OPO at 25% duty cycle. *Opt. Express* **2013**, *21*, 10062–10069. [CrossRef] [PubMed]
18. Haakestad, M.W.; Fonnum, H.; Lippert, E. Mid-infrared source with 0.2 J pulse energy based on nonlinear conversion of Q-switched pulses in $ZnGeP_2$. *Opt. Express* **2014**, *22*, 8556–8564. [CrossRef] [PubMed]
19. Liu, G.; Yang, K.; Chen, Y.; Yao, B.; Wang, R.; Mi, S.; Yang, C.; Dai, T.; Duan, X. 11.6 W middle infrared $ZnGeP_2$ optical parametric amplifier system with a 1 kHz repetition rate. *Opt Lett.* **2014**, *39*, 6589–6592. [CrossRef]
20. Qian, C.; Fan, Y.; Sun, J.; Liu, J.; Yu, T.; Shi, X.; Ye, X. High-repetition-rate 52-mJ mid-infrared laser source based on $ZnGeP_2$ MOPA system. *J. Light. Technol.* 2023, early access.
21. Qian, C.; Yao, B.; Zhao, B.; Liu, G.; Duan, X.; Ju, Y.; Wang, Y. High repetition rate 102 W middle infrared $ZnGeP_2$ master oscillator power amplifier system with thermal lens compensation. *Opt. Lett.* **2019**, *44*, 715–718. [CrossRef]

22. Liu, G.; Mi, S.; Yang, K.; Wei, D.; Li, J.; Yao, B.; Yang, C.; Dai, T.; Duan, X.; Tian, L.; et al. 161 W middle infrared $ZnGeP_2$ MOPA system pumped by 300 W-class Ho:YAG MOPA system. *Opt. Lett.* **2021**, *46*, 82–85. [CrossRef]
23. Lv, Z.; Shen, Y.; Wen, Y.; Wang, E.P.; Wang, Z.M.; Li, W.L.; Bo, Y.; Peng, Q.J. High power widely tunable mid-IR (5–7.2 μm) $ZnGeP_2$ optical parametric oscillator pumped by a 2.09 μm laser. *Infrared Phys. Technol.* **2023**, *134*, 104879. [CrossRef]
24. Qian, C.; Yu, T.; Liu, J.; Jiang, Y.; Wang, S.; Shi, X.; Ye, X.; Chen, W. A High-Energy, Narrow-Pulse-Width, Long-Wave Infrared Laser Based on ZGP Crystal. *Crystals* **2021**, *11*, 656–663. [CrossRef]
25. Qian, C.; Duan, X.; Yao, B.; Shen, Y.; Zhang, Y.; Zhao, B.; Yuan, J.; Dai, T.; Ju, Y.; Wang, Y. 11.4 W long-wave infrared source based on $ZnGeP_2$ optical parametric amplifier. *Opt. Express* **2018**, *26*, 30195–30201. [CrossRef]
26. Liu, G.Y.; Chen, Y.; Yao, B.Q.; Wang, R.X.; Yang, K.; Yang, C.; Mi, S.Y.; Dai, T.Y.; Duan, X.M. 3.5 W long-wave infrared $ZnGeP_2$ optical parametric oscillator at 9.8 μm. *Opt Lett.* **2020**, *45*, 2347–2350. [CrossRef]
27. Petrov, V.; Rotermund, F.; Noack, F.; Schunemann, P. Femtosecond parametric generation in $ZnGeP_2$. *Opt. Lett.* **1999**, *24*, 414–416. [CrossRef] [PubMed]
28. Wandel, S.; Lin, M.-W.; Yin, Y.; Xu, G.; Jovanovic, I. Parametric generation and characterization of femtosecond mid-infrared pulses in $ZnGeP_2$. *Opt. Express* **2016**, *24*, 5287–5299. [CrossRef]
29. Hinkelmann, M.; Baudisch, M.; Wandt, D.; Morgner, U.; Zawilski, K.; Schunemann, P.; Neumann, J.; Rimke, I.; Kracht, D. High-repetition rate, mid-infrared, picosecond pulse generation with μJ-energies based on OPG/OPA schemes in 2-μm-pumped $ZnGeP_2$. *Opt. Express* **2020**, *28*, 21499–21508. [CrossRef] [PubMed]
30. Grafenstein, L.; Bock, M.; Ueberschaer, D.; Escoto, E.; Koç, A.; Zawilski, K.; Schunemann, P.; Griebner, U.; Elsaesser, T. Multi-millijoule, few-cycle 5 μm OPCPA at 1 kHz repetition rate. *Opt. Lett.* **2020**, *45*, 5998–6001. [CrossRef] [PubMed]
31. Hildenbrand, A.; Kieleck, C.; Tyazhev, A.; Marchev, G.; Stöppler, G.; Eichhorn, M.; Schunemann, P.G.; Panyutin, V.L.; Petrov, V. Laser damage of the nonlinear crystals $CdSiP_2$ and $ZnGeP_2$ studied with nanosecond pulses at 1064 and 2090 nm. *Opt. Eng.* **2014**, *53*, 122511. [CrossRef]
32. Gribenyukov, A.I.; Dyomin, V.V.; Olshukov, A.S.; Podzyvalov, S.N.; Polovcev, I.G.; Yudin, N.N. Investigation of the process of laser induced damage of $ZnGeP_2$ crystals using digital holography. *Rus.Phys. J.* **2018**, *61*, 2042–2052. [CrossRef]
33. Chumside, J.H.; Wilson, J.J.; Gribenyukov, A.I.; Shubin, S.F.; Dolgii, S.I.; Andreev, Y.M.; Zuev, V.V.; Boulder, V. Frequency conversion of a CO_2 laser with ZnGeP2. In *NOAA Technical Memorandum ERL WPL-224 WPL-224WPL*; Air Resources Laboratory: Silver Spring, MD, USA, 1992; p. 18.
34. Yudin, N.N.; Antipov, O.L.; Gribenyukov, A.I.; Eranov, I.D.; Podzyvalov, S.N.; Zinoviev, M.M.; Voronin, L.A.; Zhuravleva, E.V.; Zykova, M.P. Effect of postgrowth processing technology and laser radiation parameters at wavelengths of 2091 and 1064 nm on the laser-induced damage threshold in $ZnGeP_2$ single crystal. *Quantum Electron.* **2021**, *51*, 306–316. [CrossRef]
35. Andreev, Y.M.; Badikov, V.V.; Voevodin, V.G.; Geiko, L.G.; Geiko, P.P.; Ivashchenko, M.V.; Karapuzikov, A.I.; Sherstov, I.V. Radiation resistance of nonlinear crystals at a wavelength of 9.55 μm. *Quantum Electron.* **2001**, *31*, 1075–1078. [CrossRef]
36. Peterson, R.D.; Schepler, K.L.; Brown, J.L. Damage properties of $ZnGeP_2$ at 2 mm. *J. Opt. Soc. Am. B* **1995**, *12*, 2142–2146. [CrossRef]
37. Zawilski, K.T.; Setzler, S.D.; Schunemann, P.G.; Pollak, T.M. Increasing the laser-induced damage threshold of single-crystal $ZnGeP_2$. *JOSA B* **2006**, *23*, 2310–2316. [CrossRef]
38. Zawilski, K.T.; Schunemann, P.G.; Setzler, S.D.; Pollak, T.M. Large aperture single crystal $ZnGeP_2$ for high-energy applications. *J. Cryst. Growth* **2008**, *310*, 1891–1896. [CrossRef]
39. Yudin, N.; Zinoviev, M.; Kuznetsov, V.; Slyunko, E.; Podzvalov, S.; Voevodin, V.; Lysenko, A.; Kalsin, A.; Shaimerdenova, L.; Baalbaki, H. Effect of Dopants on Laser-Induced Damage Threshold of $ZnGeP_2$. *Crystals* **2023**, *13*, 1940737. [CrossRef]
40. Guha, S.; Bartsch, M.; Hopkins, F.K.; Eaton, M.P.; Setzler, S.D.; Schunemann, P.G.; Pollak, T.M. Nonlinear absorption and laser damage threshold measurements of doped $ZnGeP_2$. *Int. Soc. Opt. Photonics* **1999**, *3793*, 9–12.
41. Peng, Y.; Wei, X.; Wang, W. Mid-infrared optical parametric oscillator based on $ZnGeP_2$ pumped by 2-μm laser. *Chin. Opt. Lett.* **2011**, *9*, 061403. [CrossRef]
42. Zinovev, M.; Yudin, N.N.; Kuznetsov, V.; Podzyvalov, S.; Kalsin, A.; Slyunko, E.; Lysenko, A.; Vlasov, D.; Baalbaki, H. High-Strength Optical Coatings for Single-Crystal $ZnGeP_2$ by the IBS Method Using Selenide and Oxide Materials. *Ceramics* **2023**, *6*, 514–524. [CrossRef]
43. Zinovev, M.; Yudin, N.N.; Kinyaevskiy, I.; Podzyvalov, S.; Kuznetsov, V.; Slyunko, E.; Baalbaki, H.; Vlasov, D. Multispectral Anti-Reflection Coatings Based on YbF_3/ZnS Materials on $ZnGeP_2$ Substrate by the IBS Method for Mid-IR Laser Applications. *Crystals* **2022**, *12*, 1932907. [CrossRef]
44. Zinoviev, M.; Yudin, N.N.; Podzvalov, S.; Slyunko, E.; Yudin, N.A.; Kulesh, M.; Dorofeev, I.; Baalbaki, H. Optical AR Coatings of the Mid-IR Band for $ZnGeP_2$ Single Crystals Based on ZnS and Oxide Aluminum. *Crystals* **2022**, *12*, 1770985. [CrossRef]
45. Kinyaevskiy, I.O.; Danilov, P.A.; Kudryashov, S.I.; Pakholchuk, P.P.; Ostrikov, S.A.; Yudin, N.N.; Zinovev, M.M.; Podzyvalov, S.N.; Andreev, Y.M. Laser-induced damage threshold of $ZnGeP_2$ crystal for (sub) picosecond 1-μm laser pulse. *Appl. Opt.* **2023**, *62*, 16–20. [CrossRef]
46. Sutowska, M.; Sutowski, P. Contemporary applications of magnetoreological fluids for finishing process. *J. Mech. Energy Eng.* **2017**, *1*, 141–152.

47. Yudin, N.; Khudoley, A.; Zinoviev, M.; Podzvalov, S.; Slyunko, E.; Zhuravleva, E.; Kulesh, M.; Gorodkin, G.; Kumeysha, P.; Antipov, O. The Influence of Angstrom-Scale Roughness on the Laser-Induced Damage Threshold of Single-Crystal $ZnGeP_2$. *Crystals* **2022**, *12*, 1505598. [CrossRef]
48. Yudin, N.; Antipov, O.; Eranov, I.; Gribenyukov, A.; Verozubova, G.; Lei, Z.; Zinoviev, M.; Podzvalov, S.; Slyunko, E.; Voevodin, V.; et al. Laser-Induced Damage Threshold of Single Crystal $ZnGeP_2$ at 2.1 µm: The Effect of Crystal Lattice Quality at Various Pulse Widths and Repetition Rates. *Crystals* **2022**, *12*, 1638422. [CrossRef]
49. Ristau, D. (Ed.) *Laser-Induced Damage in Optical Materials*; CRC Press Taylor & Francis Group: Boca Raton, FL, USA, 2015.
50. Manenkov, A.A.; Prokhorov, A.M. Laser-induced damage in solids. *Sov. Phys. Uspekhi* **1986**, *29*, 104–122. [CrossRef]
51. Kawamori, T.; Schunemann, P.G.; Gruzdev, V.; Vodopyanov, K.L. High-order (N = 4–6) multiphoton absorption and mid-infrared Kerr nonlinearity in GaP, ZnSe, GaSe, and ZGP crystals. *APL Photon.* **2022**, *7*, 086101. [CrossRef]
52. Antipov, O.L.; Kositsyn, R.I.; Eranov, I.D. 36W Q-switched Ho^{3+}: YAG laser at 2097 nm pumped by a Tm fiber laser: Evaluation of different Ho^{3+} doping concentrations. *Laser Phys. Lett.* **2017**, *14*, 015002. [CrossRef]
53. "The R-on-1 Test", Lidaris LIDT Service. 2019. Available online: http://lidaris.com/laserdamage-testing/ (accessed on 16 November 2020).
54. Lei, Z.; Okunev, A.O.; Zhu, C.; Verozubova, G.A.; Yang, C. Imaging of microdefects in $ZnGeP_2$ single crystals by X-ray topography. *J. Cryst. Growth* **2020**, *534*, 125487–125492. [CrossRef]
55. Lei, Z.; Okunev, A.O.; Zhu, C.; Verozubova, G.A.; Ma, T.; Yang, C. Photoelasticity method for study of structural imperfection of $ZnGeP_2$ crystals. *J. Cryst. Growth* **2016**, *450*, 34–38. [CrossRef]
56. Yudin, N.; Antipov, O.; Balabanov, S.; Eranov, I.; Getmanovskiy, Y.; Slyunko, E. Effects of the Processing Technology of CVD-ZnSe, Cr^{2+}:ZnSe, and Fe^{2+}:ZnSe Polycrystalline Optical Elements on the Damage Threshold Induced by a Repetitively Pulsed Laser at 2.1 µm. *Ceramics* **2022**, *5*, 459–471. [CrossRef]
57. Gribenykov, A.I.; Verozubova, G.A.; Trofimov, A.; Yunda, N.T.; Vere, A.W.; Flyun, C.J. Native Point Defect Interactions in ZGP Crystals under Influence of e-Beam Irradiation. *MRS Online Proceedings Library.* **2002**, *744*, 540. [CrossRef]
58. Grigorieva, V.S.; Prochukhan, V.D.; Rud, Y.V.; Yakovenko, A.A. About doping of the semiconductor compound $ZnGeP_2$. Doped Semiconductors M.: "Science", 1975; pp. 8–11.
59. Voevodin, V.G. Optical Electronics Elements Based on A2B4C2 Compounds: Preparation, Properties and Application. Ph.D. Thesis, Sciences, Siberian Institute of Physics and Technology, Tomsk, Russia, 2003; p. 395.
60. Schnars, U.; Juptner, W. *Digital Hologram Recording, Numerical Reconstruction, and Related Techniques*; Springer: Berlin, Germany, 2005; p. 164.
61. Collier, R.; Burkhart, K.; Lin, L. *Optical Holography*; Academic Press: New York, NY, USA, 1979; Volume 13, p. 686.
62. Dyomin, V.V.; Polovcev, I.G.; Kamenev, D.V. The internal defects detection in crystals by digital holographic methods. Conference Series. *J. Phys.* **2016**, *737*, 012072.
63. Buehler, E.; Wernick, J.H. Concerning growth of single crystals of the II-IV-V diamond-like compounds ZnSiP2, CdSiP2, ZnGeP2, and CdSnP2 and standard enthalpies of formation for ZnSiP2 and CdSiP2. *J. Cryst. Growth* **1971**, *8*, 324–332. [CrossRef]
64. Piotrowski, M.; Medina, M.A.; Schellhorn, M.; Mueller, C.; Spindler, G.; Hildenbrand-Dhollande, A. Experimental and numerical studies of thermal lensing and gain guiding effects in a high-power ZGP OPO. In Proceedings of the 2021 Conference on Lasers and Electro-Optics Europe and European Quantum Electronics Conference, Munich, Germany, 21–25 June 2021. Technical Digest of CLEO Europe-EQEC 2021, paper ca_8_6.
65. Crisp, M.D. Laser-Induced Surface Damage of Transparent Dielectrics. *IEEE J. Quantum Electron.* **1974**, *10*, 57–62. [CrossRef]
66. Antipov, O.L.; Eranov, I.D.; Kositsyn, R.I. 10-W mid-IR optical parametric oscillators based on $ZnGeP_2$ elements pumped by a fibre-laser-pumped Ho: YAG Laser. Experimental and numerical study. *Quantum Electron.* **2017**, *47*, 601. [CrossRef]
67. Antipov, O.; Dobrynin, A.; Getmanovskiy, Y.; Karaksina, E.; Shiryaev, V.; Sukhanov, M.; Kotereva, T. Thermal Lensing and Laser-Induced Damage in Special Pure Chalcogenide $Ge_{35}As_{10}S_{55}$ and $Ge_{20}As_{22}Se_{58}$ Glasses under Quasi-CW Fiber Laser Irradiation at 1908 nm. *Photonics* **2023**, *10*, 252. [CrossRef]
68. Available online: http://refractiveindex.info (accessed on 27 November 2023).
69. Yudin, N.N.; Vlasov, D.V.; Antipov, O.L.; Gribenyukov, A.I.; Zinoviev, M.M.; Podzyvalov, S.N.; Slyunko, E.S.; Yudin, N.A.; Kulesh, M.M.; Kuznetsov, V.S.; et al. Visualization and Characterization of Pre-breakdown Processes in the Volume of a $ZnGeP_2$ Single Crystal During Parametric Generation of Radiation in the Wavelength Range of 3.5–5 µm when Pumped by Ho:YAG Laser Radiation. *Russ. Phys. J.* **2023**, *65*, 2130–2136. [CrossRef]